Earth and Planetary Science Letters 434 (2016) 75–90

Contents lists available at ScienceDirect

Earth and Planetary Science Letters

www.elsevier.com/locate/epsl

Late Neogene oroclinal bending in the central Taurides: A record of terminal eastward subduction in southern Turkey?

Ayten Koç [a,b,*], Douwe J.J. van Hinsbergen [a], Nuretdin Kaymakci [c], Cornelis G. Langereis [a]

[a] Department of Earth Sciences, Utrecht University, 3508 TA Utrecht, The Netherlands
[b] Department of Geological Engineering, Yüzüncü Yıl University, Van, 65080, Turkey
[c] Department of Geological Engineering, Middle East Technical University, Ankara, 06531, Turkey

ARTICLE INFO

Article history:
Received 14 June 2015
Received in revised form 10 November 2015
Accepted 14 November 2015
Available online 2 December 2015
Editor: A. Yin

Keywords:
paleomagnetism
Miocene marine basins
subduction
oroclinal bending
Isparta Angle
Taurides

ABSTRACT

The Tauride fold-thrusts belt formed during ~S–N convergence between Africa and Eurasia since Cretaceous time. The western end of the central Taurides strike NW–SE, highly obliquely to the overall convergence direction, and connect to the NE–SW Beydağları–Lycian Nappe flank of the western Taurides, forming the so-called 'Isparta Angle'. In Neogene time, the western and central Taurides and the inner part of the Isparta Angle became overlain by Neogene sedimentary basins including Manavgat, Köprüçay and Aksu, characterized by marine clastics and carbonates. The eastern limb of the Isparta Angle experienced multidirectional Miocene to Present extension, whereas E–W shortening affected the marine sedimentary basins in the heart of the Isparta Angle. To quantitatively reconstruct the Neogene kinematic evolution of the Taurides, towards restoring the subduction system accommodating Africa–Eurasia convergence, we paleomagnetically assess if and when vertical axis rotations affected the Manavgat, Köprüçay, and Aksu basins in Early Miocene to Pliocene times. We show that the northern Köprüçay Basin rotated ~20–30° clockwise, the Manavgat Basin underwent ~25–35° counterclockwise rotation, and the Aksu Basin underwent no rotation since the Early-Middle Miocene. It was previously shown that the Beydağları region underwent a post-Middle Miocene ~20° counterclockwise rotation. These results show that the prominent oroclinal salient geometry of the western Taurides thus acquired, at least in part, since Miocene times, that the Köprüçay Basin rotated relative to the Aksu Basin along the Aksu thrust, and that the Beydağları platform rotated relative to the Aksu Basin along the Bucak thrust, which must have both been active until Late Neogene time. This synchronous E–W shortening in the heart of the Isparta Angle, and multidirectional extension in its eastern limb may be explained by relative westward retreat of an eastward dipping subducting Antalya slab that has previously been imaged by seismic tomography and a Benioff zone. The Neogene Bucak thrust west of the Aksu Basin may represent the most recent surface expression of the Antalya subduction zone.

1. Introduction

The Isparta Angle (IA) is a triangular-shaped morpho-tectonic structure defined by the change in strike of the Tauride fold and thrust belt in southern Turkey, containing regionally extensive Mesozoic platform carbonate sequences. It was first defined by Blumenthal (1963) and is located at the intersection of the southward-convex Aegean and Cyprus arcs (Fig. 1a). The thin-skinned Central Tauride fold-thrust belt forms the eastern limb and overthrusts the autochthonous Beydağları platform to the west. The Lycian Nappes form the western limb and overthrust the Beydağları platform to the southeast (Fig. 1b). The carbonate thrust slices of the Central Taurides in the east are overlain by (meta)sedimentary nappes and ultimately, ophiolites. Thrusting occurred continuously or intermittently from Late Cretaceous to Neogene time (Şengör and Yılmaz, 1981; Hayward, 1984; Collins and Robertson, 2003; Poisson et al., 2003; van Hinsbergen, 2010).

After thrusting and folding, the Central Taurides became overprinted since Miocene times by multi-directional extension with major basin-bounding faults accommodating (N)E–(S)W extension (Koç et al., 2012, 2015). Interestingly, this occurred contemporaneously with E–W shortening accommodated by N–S striking folds and thrusts in the heart of the Isparta Angle (Poisson et al., 2003; Çiner et al., 2008; Hall et al., 2014). Here, marine sediments are exposed that were accumulated in basins known as the Aksu, Köprüçay and Manavgat basins (Fig. 1c), which uncon-

* Corresponding author at: Department of Geological Engineering, Yüzüncü Yıl University, Van, 65080, Turkey.
E-mail address: aytenkoc@yyu.edu.tr (A. Koç).

http://dx.doi.org/10.1016/j.epsl.2015.11.020
0012-821X/

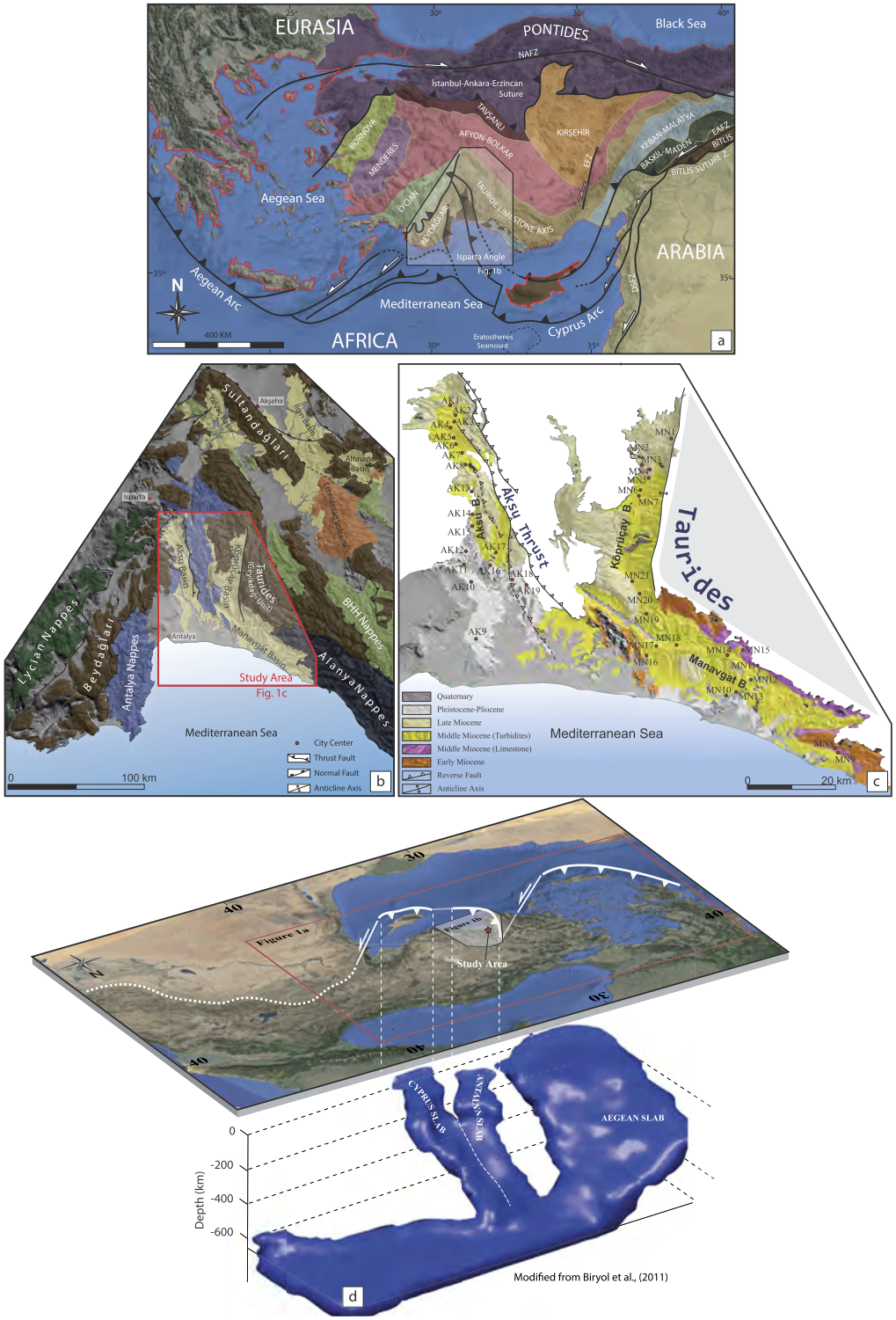

Fig. 1. (a) Simplified structural map and major tectonic zone of Turkey overlain on an SRTM topographic image. (b) Major tectonic structures and units in the Isparta Angle. (c) Simplified geological map of the study area, numbers indicate the paleomagnetic site locations. (d) 3-D diagram of the segmented geometry of the subducting African lithosphere beneath Anatolia inferred from tomographic model (modified from Biryol et al. (2011)). NAFZ: North Anatolian Fault Zone, EAFZ: East Anatolian Fault Zone, EFZ: Ecemiş Fault Zone, BHH: Beyşehir–Hoyran–Hadim Nappes.

formably cover the Tauride carbonates. The Aksu Thrust delimiting the eastern margin of the Aksu Basin exemplifies Miocene to Pliocene E–W to NE–SW directed thrusting in the core of the Isparta Angle (Glover and Robertson, 1998; Poisson et al., 2003; Deynoux et al., 2005; Flecker et al., 2005; Çiner et al., 2008) and together with its offshore equivalents in the Bay of Antalya indicates that the youngest compressional tectonic event in the heart of the Isparta Angle lasted until the Pliocene (Poisson et al., 2003) or even into the Quaternary (Hall et al., 2014) (Fig. 1a and 1b).

E–W Miocene thrusting is restricted to the heart of the Isparta Angle, and is not prominent elsewhere in south Anatolia. Previous workers postulated a causal relationship between compression in the Isparta Angle and westwards motion of Anatolia relative to Eurasia (Şengör et al., 1985; Deynoux et al., 2005;

Glover and Robertson, 1998; Hall et al., 2014), as distinctly shown in GPS-derived velocity fields (Reilinger et al., 2006, 2010). This shortening is thought to be closely related to the Arabia–Eurasia collision in eastern Turkey (Şengör et al., 2003; Faccenna et al., 2006; Hüsing et al., 2009; Okay et al., 2010). Linking shortening in the heart of the Isparta Angle to a push from the east, however, is problematic in the light of evidence for the synchronous E–W extension component deforming the eastern limb of the Isparta Angle (Koçyiğit et al., 2000; Schildgen et al., 2012a, 2012b; Koç et al., 2012, 2015). The present-day tectonic regime as portrayed by active seismicity, earthquake focal mechanism solutions, field data, including fault slip data and GPS measurements show that the northern apex and eastern limb of the Isparta Angle experience extension (Koçyiğit and Özacar, 2003; Reilinger et al., 2006; Kalyoncuoğlu et al., 2011; Koç et al., 2012, 2015). The >21 km high topography formed by thrusted carbonates of the Central Taurides is flanked by Neogene continental basins. These formed in an overriding plate setting of the present-day subduction zone consuming the African plate, and are characterized by thick accumulations of continental sediments and volcanics (Koç et al., 2012, 2015). Fault slip mechanism solutions of moderate-size earthquakes indicate regional extension (Taymaz et al., 2004; Ergin et al., 2009; Tiryakioğlu et al., 2013; Poyraz et al., 2014), with range and basin-bounding major normal faults accommodating multiple directions of extension in tri-axial strain conditions. Similarly, paleostress inversion studies on the Altınapa and Yalvaç basins from the eastern limb and the northern tip of the Isparta Angle, respectively, show that multi-directional extension prevailed since Middle Miocene times (Koçyiğit et al., 2000; Schildgen et al., 2012a, 2012b; Koç et al., 2012, 2015).

Here we provide results of an extensive paleomagnetic survey constraining vertical axis rotations in the Aksu, Köprüçay and Manavgat basins since the Neogene to explore how extension and contraction at short distances in the Isparta Angle area can kinematically be linked and what could be the common cause of this complex deformation in the region. Then, we will discuss these results within the context of the dynamics of subducted slabs of African lithosphere that were previously imaged by seismic tomography below southwestern Turkey (Biryol et al., 2011), immediately below the study area (Fig. 1d).

2. Geological setting

Intense deformation in Anatolia occurred in response to long-lived and ongoing convergence between Africa and Eurasia. Today, Anatolia is located in the overriding plate of a complex subduction system with curved trenches forming the Aegean and Cyprus arcs (Fig. 1a). The junction between these arcs forms the so-called Isparta Angle (Blumenthal, 1963), which is characterized by a long-term polyphase deformation history (Glover and Robertson, 1998; Poisson et al., 2003; Robertson et al., 2003; Van Hinsbergen et al., 2010a, 2010b; van Hinsbergen and Schmid, 2012). The lowest structural unit exposed in the Isparta Angle area is the Beydağları platform, overthrusted from the northwest by the Lycian nappes (i.e. the western Tauride fold-thrust belt), and from the east by the Central Tauride fold-thrust belt (Fig. 1b). The deformation history of the Isparta Angle is further complicated by the so-called Antalya and Alanya Nappes (Fig. 1b) that overthrust the Taurides from the south in late Cretaceous time (Poisson et al., 2003). These nappes comprise a series of Paleozoic and Mesozoic passive margin sediments, volcanics and ophiolites (Robertson and Woodcock, 1982), that after their emplacement in the late Cretaceous became passive riders on the Tauride autochthon, and became incorporated in the west-verging fold-thrust belt of the Central Taurides since the Eocene (Özgül, 1984).

The final emplacement of the Lycian Nappes over the Beydağları platform occurred during the Early Miocene (Hayward, 1984; Okay, 1989; Collins and Robertson, 2003; van Hinsbergen et al., 2010a; van Hinsbergen, 2010), after which they together underwent ~20° counterclockwise rotation (Kissel and Poisson, 1987; Morris and Robertson, 1993; Van Hinsbergen et al., 2010a, 2010b), kinematically linked to oroclinal bending and back-arc extension in the Aegean region (van Hinsbergen and Schmid, 2012).

The Central Taurides fold-and-thrust belt developed from the Late Cretaceous until after the Middle Eocene, as shown by the youngest deposits within the belt on the structurally lowest platform sequence units known as the Geyikdağı unit (Fig. 1b). This unit is generally considered as the thrusted equivalent of the Beydağları unit (Özgül, 1976) ('para-autochthon'). It is overthrusted from the east by higher nappes (Beyşehir–Hoyran–Hadim nappes) that include Upper Paleozoic–Upper Cretaceous platform carbonates, marginal and deep marine sediments and volcanics, and eventually ophiolites and related mélanges (Özgül, 1984; Andrew and Robertson, 2002). A paleomagnetic study by Kissel et al. (1993) and later Meijers et al. (2011) showed that some of these nappes underwent clockwise rotation of about 40° since the Eocene.

Thrusting in the heart of the Isparta Angle did not stop in the Eocene, but either continued, or was reactivated, in the Middle Miocene to Pliocene, as constrained from marine sediments in the Aksu Basin (Fig. 1c). These are overthrusted along the Aksu Thrust by Geyikdağı and overlying Antalya Nappes rocks (Glover and Robertson, 1998; Poisson et al., 2003; Deynoux et al., 2005; Flecker et al., 2005; Çiner et al., 2008). Shortening is evident from strong folding and thrusting of the Lower to uppermost Miocene stratigraphy in the Aksu and Köprüçay basins (Glover and Robertson, 1998; Poisson et al., 2003; Karabıyıkoğlu et al., 2005; Çiner et al., 2008), alongside major slumping.

3. Paleomagnetic sampling and analysis

3.1. Paleomagnetic sampling

In total, 520 oriented cores were sampled at 40 sites distributed within Miocene–Pliocene marine sedimentary rocks from the basins in the heart of the Isparta Angle. We sampled fresh outcrops of sedimentary rock away from brittle faults to minimalize measuring rotations reflecting local deformation. Nineteen sampling sites were located in the Aksu Basin (Fig. 1c) and twenty-one sampling sites are distributed within the Köprüçay and Manavgat basins (Fig. 1c) in Lower to Upper Miocene sediments. Samples were taken from limestone, silt and claystone, and few sandstones, deposited in marine environments. Samples were drilled using a gasoline powered motor drill and sample orientations were measured with a magnetic compass. Sample orientations as well as bedding attitudes were corrected for present day declination (+4.5°). At least 10 standard oriented cores were collected from each site after removing the weathered surface of the outcrop. In the laboratory, samples were cut into standard specimens, providing in most cases two or more specimens per core (referred to as A and B specimens, for deeper and shallower parts of the core, respectively).

3.2. Paleomagnetic analyses

To determine magnetic carriers of the ChRM in the samples, thermomagnetic runs were carried out in air (Fig. 2), using a modified horizontal translation type Curie balance, with a sensitivity of $\sim 5 \times 10^{-9}$ Am^2 (Mullender et al., 1993). Approximately 50–100 mg of powdered rock sample (depending on the magnetic intensity of the sample) was put into a quartz-glass sample holder held in place by quartz wool. The measurement procedure consists of a

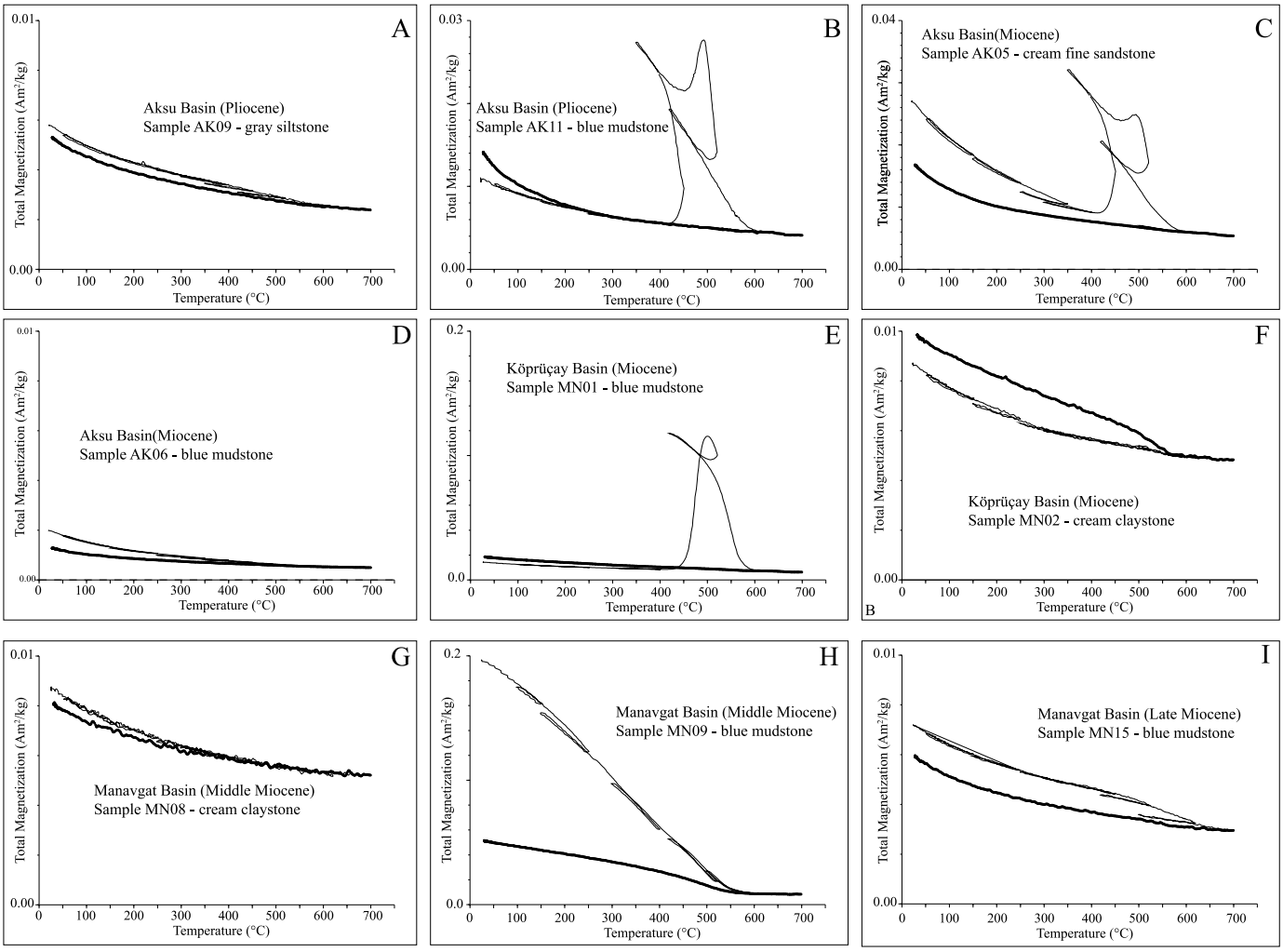

Fig. 2. Thermomagnetic curve generated with the segmented heating protocol (Mullender et al., 1993) for representative samples. The final cooling segment is indicated with thicker black line. A noisy appearance is indicative of a weak magnetic signal. See for text for explanation of the thermomagnetic behavior.

number of heating and cooling cycles up to a maximum 700 °C with 10 °C/min rates.

A total of 534 specimens were demagnetized (Table 1). Thermal (TH) stepwise demagnetization of 169 specimens (in 10–20 steps from room temperature up to 400–680 °C depending on the maximum unblocking temperature) was performed to verify the reproducibility of alternating field (AF) demagnetization performed on 365 specimens (16 steps from 0 to 100 mT). AF demagnetization was carried out in an in-house developed robotized 2G DC SQUID magnetometer (noise level 3×10^{-12} Am^2), which provides significantly better results on samples with low natural remanent magnetization (NRM) intensity. As a rule, specimens were heated to 150 °C to remove possible stress caused by weathering (van Velzen and Zijderveld, 1995).

Stepwise demagnetization of the NRM is displayed in orthogonal vector diagrams (Fig. 3) (Zijderveld, 1967). Magnetization components were determined using principle component analysis (Kirschvink, 1980) on approximately five to seven successive temperature or AF steps in the majority of the specimens. A great circle approach (McFadden and McElhinny, 1988) was used when the samples yielded directions intermediate between those of two (different) components with overlapping temperature or coercivity spectra (Fig. 3). This method iteratively determines the direction in the plane (great circle) that lies closest to the mean direction of well-determined NRM directions (set points) and great circle solutions.

Site mean directions according to statistical procedures detailed in Deenen et al. (2011), virtual geomagnetic poles (VGP) and their statistical properties were calculated from the ChRM directions (Fig. 4). A fixed cut-off (45°) was applied on the VGP distributions and corresponding directions were rejected. The error in declination (ΔD_x) and inclination (ΔI_x) were calculated separately from A_{95} (the 95% cone of confidence of VGPs) following Butler (1992); minimum and maximum values of A_{95} that are consistent with secular variation are according to Deenen et al. (2011) (Fig. 4).

To assess whether two distributions have a common true mean direction (CTMD), we used the reversal test developed by McFadden and McElhinny (1990) and their classifications (A, B, C and indeterminate). The classifications are based on the critical angle γ_c and the angle γ between the means. As a rule, we used (Monte Carlo) simulation, thereby effectively applying the Watson (1983) statistic test. We performed the test on the VGP distributions because those are more Fisherian than the ChRM distributions (Deenen et al., 2011) (Fig. 4). To test the primary origin of the ChRM, fold tests at 95% confidence interval were performed on the regional datasets by combining site-mean directions from several paleomagnetic sites within a general area and age window (Tauxe and Watson, 1994).

Table 1
Table showing all paleomagnetic data from this study.

	Lat	Long	Age	N	ChRM directions – in situ									Strike/Dip	ChRM directions – tilt corrected								
					N_{45}	D	I	ΔD_x	ΔI_x	k	α_{95}	K	$A_{95\,min} < A_{95} < A_{95\,max}$		N_{45}	Dec	Inc	ΔD_x	ΔI_x	k	α_{95}	K	$A_{95\,min} < A_{95} < A_{95\,max}$
Aksu Basin (AB-Pliocene)																							
AK09	36.9715	30.8199	Pliocene	10	10	8.2	37.4	9.7	13.1	30.0	9.0	29.3	$4.8 < 9.1 < 19.2$	000/00									
AK10	37.1161	30.8073	Pliocene	13	13	170.9	−42.3	10.0	12.0	17.0	10.4	21.8	$4.3 < 9.1 < 16.3$	000/00									
AK11	37.1595	30.7902	Pliocene	15	15	181.2	−44.3	1.9	2.2	599.6	1.6	483.5	$\mathbf{1.7} < A_{95\,min}$ (4.1)	000/00									
AK12	37.1925	30.7945	Pliocene	15	15	357.0	51.7	4.1	3.7	187.3	2.8	125.5	$\mathbf{3.4} < A_{95\,min}$ (4.1)	000/00									
AK18	37.1210	30.9107	Pliocene	14	13	185.0	−56.4	12.5	9.5	29.1	7.8	18.4	$4.3 < 9.9 < 16.3$	000/00									
Mean (N)				**30**	**29**	**003.5**	**50.1**	**5.8**	**5.5**	**33.5**	**4.7**	**30.1**	$\mathbf{3.1 < 5.0 < 9.8}$										
Mean (R)				**37**	**36**	**176.3**	**−44.0**	**4.0**	**4.6**	**38.9**	**3.9**	**45.0**	$\mathbf{2.9 < 3.6 < 8.6}$										
Mean (N + R)				**67**	**65**	**359.3**	**46.8**	**3.5**	**3.7**	**34**	**3.1**	**34.2**	$\mathbf{2.3 < 3.1 < 5.9}$										
Aksu Basin (AB-North)																							
AK01	37.5609	30.7550	Miocene	15	15	9.6	43.9	6.3	7.2	47.7	5.6	46.9	$4.1 < 5.6 < 14.9$	101/18	15	8.8	61.9	10.4	6.3	47.7	5.6	26.6	$4.1 < 7.6 < 14.9$
AK02	37.5364	30.7680	Miocene	15	15	345.8	53.8	6.6	5.6	87.6	4.1	49.8	$4.1 < 5.5 < 14.9$	200/14	15	333.4	44.6	5.5	6.2	87.7	4.1	61.4	$4.1 < 4.9 < 14.9$
AK03	37.5195	30.7651	Miocene	15	15	14.0	54.4	3.2	2.7	324.0	2.6	209.6	$2.6 < A_{95\,min}$ (4.1)	275/18	15	11.5	36.6	2.2	3.1	324.5	2.1	334.9	$2.1 < A_{95\,min}$ (4.1)
AK04*	37.5054	30.7552	Miocene	13	13	178.8	−41.4	6.9	8.5	43.1	6.4	43.8	$4.3 < 6.3 < 16.3$	230/07	13	175.4	35.8	6.2	8.7	43.1	6.4	50.9	$4.3 < 5.9 < 16.3$
AK05*	37.4791	30.7629	Miocene	14	14	3.2	48.2	7.1	7.2	42.0	6.2	42.4	$4.2 < 6.2 < 15.6$	230/07	14	357.9	43.5	6.5	7.6	42.0	5.9	46.4	$4.1 < 5.9 < 15.6$
AK06	37.4631	30.7691	Miocene	14	14	359.3	54.5	7.5	6.2	71.4	4.7	43.2	$4.2 < 6.1 < 15.6$	235/04	14	356.4	51.2	6.9	6.4	71.5	4.7	47.1	$4.2 < 5.9 < 15.6$
AK07	37.4414	30.7850	Miocene	15	15	13.5	50.4	5.5	5.2	100.3	3.8	68.0	$4.1 < 4.7 < 14.9$	300/23	15	18.2	28.1	3.9	6.2	100.2	3.8	105.6	$\mathbf{3.7} < A_{95\,min}$ (4.1)
AK08	37.4119	30.7934	Miocene	13	12	332.7	51.8	9.2	8.3	49.1	6.3	32.5	$4.4 < 7.7 < 17.1$	300/16	12	345.9	41.6	7.6	9.3	49.2	6.3	39.7	$4.4 < 7.0 < 17.1$
Mean (N)				**97**	**96**	**000.7**	**52.3**	**3.3**	**2.9**	**44.3**	**2.2**	**28.4**	$\mathbf{1.9 < 2.8 < 4.6}$		**97**	**359.1**	**45.3**	**3.9**	**4.3**	**21.9**	**3.1**	**18.0**	$\mathbf{1.9 < 3.5 < 4.6}$
Mean (R)				**16**	**16**	**183.3**	**−39.7**	**6.7**	**8.5**	**36.6**	**6.2**	**36.9**	$\mathbf{4.0 < 6.2 < 14.3}$		**16**	**179.7**	**−34.7**	**6.0**	**8.6**	**36.9**	**6.2**	**43.0**	$\mathbf{4.0 < 5.7 < 14.3}$
Mean (N + R)				**113**	**112**	**1.2**	**50.5**	**3.0**	**2.8**	**38.5**	**2.2**	**27.9**	$\mathbf{1.8 < 2.6 < 4.2}$		**113**	**359.2**	**43.8**	**3.5**	**4.0**	**22.3**	**2.9**	**19.2**	$\mathbf{1.8 < 3.1 < 4.2}$
Aksu Basin (AB-South)																							
AK13	37.3429	30.8080	Miocene	15	15	217.0	−75.0	19.0	5.3	56.6	5.1	19.7	$4.1 < 8.8 < 14.9$	256/21	15	188.0	−57.5	8.5	6.2	56.7	5.1	33.5	$4.1 < 6.7 < 14.9$
AK14	37.2857	30.8110	Miocene	13	13	344.0	52.9	6.2	5.4	90.5	4.3	65.8	$4.3 < 5.1 < 16.3$	190/36	13	318.5	29.3	3.9	6.1	90.4	4.4	124.7	$3.7 < A_{95\,min}$ (4.3)
AK15	37.2560	30.8104	Miocene	10	10	182.2	−45.8	8.2	8.9	63.2	6.1	45.2	$4.8 < 7.3 < 19.2$	000/00	10	182.2	−45.8	8.2	8.9	63.2	6.1	45.2	$4.8 < 7.3 < 19.2$
AK16	37.1577	30.8550	Miocene	13	13	004.7	55.4	6.5	5.2	117.5	3.8	62.5	$4.3 < 5.3 < 16.3$	098/08	13	3.9	63.4	8.3	4.7	117.7	3.8	50.6	$4.3 < 5.9 < 16.3$
AK17	37.1900	30.8697	Miocene	15	15	14.1	53.6	6.2	5.3	78.2	4.4	56.4	$4.1 < 5.1 < 14.9$	286/21	15	14.7	32.6	4.1	17.8	78.2	4.4	97.1	$\mathbf{3.9} < A_{95\,min}$ (4.1)
AK19	37.1072	30.9468	Miocene	9	9	216.1	−42.3	9.0	10.8	39.6	8.3	40.3	$5.0 < 8.2 < 20.5$	166/26	9	190.4	−58.6	14.3	10.0	39.5	8.3	22.9	$5.0 < 11.0 < 20.5$
Mean (N)				**41**	**41**	**001.5**	**54.6**	**5.0**	**4.1**	**52.5**	**3.1**	**31.3**	$\mathbf{2.7 < 4.1 < 7.9}$										
Mean (R)				**34**	**33**	**203.1**	**−57.9**	**10.5**	**7.6**	**15.8**	**6.5**	**10.3**	$\mathbf{3.0 < 8.2 < 9.1}$		**34**	**186.5**	**−54.4**	**5.7**	**4.7**	**43.0**	**3.8**	**28.7**	$\mathbf{2.9 < 4.7 < 8.9}$
Mean (N + R)				**75**	**73**	**10.5**	**56.1**	**5.6**	**4.4**	**23.6**	**3.5**	**14.5**	$\mathbf{2.2 < 4.5 < 5.5}$										
Köprüçay Basin (KB-North)																							
MN01	37.4772	31.3124	Miocene	10	10	22.9	54.7	11.2	9.1	35.0	8.3	29.1	$4.8 < 9.1 < 19.2$	275/14	10	18.7	41.2	8.1	10.1	35.0	8.3	43.0	$4.8 < 7.5 < 19.2$
MN02	37.4394	31.2122	Miocene	7	7	217.9	−49.4	8.9	8.7	76.5	6.9	63.0	$5.5 < 7.7 < 24.1$	290/20	7	213.4	−30.2	6.4	10.0	76.7	6.9	97.4	$5.5 < 6.1 < 24.1$
MN03	37.4109	31.2392	Miocene	9	9	8.5	51.2	13.5	12.5	34.0	9.0	21.1	$5.0 < 11.5 < 20.5$	071/14	9	20.5	63.0	19.0	10.9	33.9	9.0	15.6	$5.0 < 13.5 < 20.5$
MN04	37.3992	31.2589	Miocene	11	11	176.3	−62.4	9.0	5.3	98.7	4.6	50.9	$4.6 < 6.5 < 18.1$	354/25	11	214.2	−52.7	7.2	6.3	98.6	4.6	58.1	$4.6 < 6.0 < 18.1$
MN05	37.3778	31.2562	Miocene	12	12	19.0	43.1	4.8	5.7	85.2	4.7	99.5	$4.4 = A_{95\,min}$ (4.4)	163/18	12	1.5	51.5	5.8	5.3	85.0	4.7	78.8	$4.4 < 4.9 < 17.1$
MN06	37.3469	31.2342	Miocene	12	12	12.1	29.3	7.6	11.9	34.9	7.5	36.5	$4.4 < 7.3 < 17.1$	000/00	12	12.1	29.3	7.6	11.9	34.9	7.5	36.5	$4.4 < 7.3 < 17.1$
MN07	37.3329	31.2307	Miocene	10	10	0.2	38.0	7.1	9.5	46.7	7.1	53.9	$4.8 < 6.6 < 19.2$	140/08	10	354.8	42.9	7.7	9.1	46.7	7.1	48.6	$4.8 < 7.0 < 19.2$
Mean (N)				**53**	**53**	**12.2**	**42.9**	**4.4**	**5.2**	**25.6**	**3.9**	**25.1**	$\mathbf{2.5 < 4.0 < 6.7}$		**52**	**008.0**	**44.8**	**4.7**	**5.3**	**22.6**	**4.2**	**22.6**	$\mathbf{2.5 < 4.2 < 6.8}$
Mean (R)				**18**	**18**	**195.9**	**−59.1**	**11.6**	**8.0**	**27.6**	**6.7**	**16.1**	$\mathbf{3.8 < 8.9 < 13.3}$		**18**	**213.8**	**−44.0**	**6.1**	**7.0**	**33.6**	**6.1**	**40.4**	$\mathbf{3.8 < 5.5 < 13.3}$
Mean (N + R)				**71**	**71**	**12.9**	**47.0**	**4.4**	**4.7**	**22.1**	**3.7**	**19.7**	$\mathbf{2.2 < 3.9 < 5.6}$		**71**	**15.2**	**45.4**	**4.6**	**5.1**	**19.6**	**3.9**	**17.6**	$\mathbf{2.2 < 4.1 < 5.6}$
Köprüçay Basin (KB-South)																							
MN19	37.0349	31.2489	Miocene						No Reliable Result					002/53					No Reliable Result				
MN20	37.0860	31.2329	Miocene						No Reliable Result					120/24					No Reliable Result				
MN21	37.1179	31.2146	Miocene						No Reliable Result					105/32					No Reliable Result				
Manavgat Basin (MB-West)																							
MN16	36.9295	31.2501	Miocene						No Reliable Result					242/25					No Reliable Result				
MN17	36.9535	31.2743	Miocene						No Reliable Result					239/20					No Reliable Result				
MN18	36.9565	31.3262	Miocene						No Reliable Result					302/24					No Reliable Result				

(*continued on next page*)

Table 1 (*continued*)

	Lat	Long	Age	N	ChRM directions – in situ									Strike/Dip	ChRM directions – tilt corrected								
					N_{45}	D	I	ΔD_x	ΔI_x	k	α_{95}	K	$A_{95\,min} < A_{95} < A_{95\,max}$		N_{45}	Dec	Inc	ΔD_x	ΔI_x	k	α_{95}	K	$A_{95\,min} < A_{95} < A_{95\,max}$
Manavgat Basin (MB-Mid)																							
MN10*	36.8287	31.4509	L. Miocene	9	9	347.3	48.1	7.9	8.1	73.1	6.1	56.7	$5.0 < 6.9 < 20.5$	170/02	9	345.0	48.0	7.8	8.0	73.1	6.1	58.5	$5.0 < 6.8 < 20.5$
MN11	36.9049	31.5304	L. Miocene	10	9	188.2	−30.7	14.1	21.7	13.4	14.6	15.6	$5.0 < 13.5 < 20.5$	128/32	9	168.2	−56.0	22.9	17.7	13.4	14.6	9.0	$5.0 < 18.2 < 20.5$
MN12	36.8685	31.5138	L. Miocene	9	9	349.2	40.2	11.1	14.0	24.2	10.7	26.5	$5.0 < 10.2 < 20.5$	128/12	9	339.9	47.4	13.0	13.6	24.2	10.7	21.3	$5.0 < 11.4 < 20.5$
MN13	36.8377	31.4772	L. Miocene	6	6	354.9	51.5	10.9	10.0	89.4	7.1	53.9	$5.9 < 9.2 < 26.5$	204/10	6	345.4	45.9	9.9	10.7	89.2	7.1	59.3	$5.9 < 8.8 < 26.5$
MN14	36.9309	31.4546	L. Miocene	No Reliable Result										140/21	No Reliable Result								
MN15	36.9424	31.4941	L. Miocene	12	12	352.4	55.1	4.7	3.8	181.4	3.2	132.3	**$3.8 < A_{95\,min}$ (4.4)**	235/06	12	349.0	49.7	4.0	3.9	181.1	3.2	160.2	**$3.4 < A_{95\,min}$ (4.4)**
Mean (N)				**33**	**33**	**352.1**	**49.7**	**4.2**	**4.1**	**48.4**	**3.6**	**49.3**	**$3.0 < 3.6 < 9.1$**		**33**	**346.3**	**48.6**	**4.1**	**4.2**	**60.2**	**3.2**	**49.2**	**$3.0 < 3.6 < 9.1$**
Mean (R)				**13**	**12**	**180.7**	**−34.5**	**13.2**	**19.0**	**12.6**	**12.7**	**13.0**	**$4.4 < 12.5 < 17.1$**		**11**	**159.2**	**−50.9**	**14.3**	**13.3**	**19.5**	**10.6**	**15.1**	**$4.6 < 12.2 < 18.1$**
Mean (N + R)				**46**	**44**	**353.4**	**46.1**	**4.4**	**4.8**	**27.2**	**4.2**	**30.9**	**$2.6 < 3.9 < 7.6$**		**44**	**344.6**	**49.2**	**4.5**	**4.5**	**40.0**	**3.4**	**31.3**	**$2.6 < 3.9 < 7.6$**
Manavgat Basin (MB-East)																							
MN08 (N)	36.6943	31.7259	M. Miocene	11	11	351.6	37.6	5.0	6.7	81.9	5.1	96.6	$4.6 < 4.7 < 18.1$	105/18	11	342.9	53.6	7.2	6.1	81.9	5.1	59.9	$4.6 < 5.9 < 18.1$
MN09 (R)	36.6840	31.7334	M. Miocene	11	6	173.1	47.2	6.9	7.2	136.9	5.7	124.3	$5.9 < 6.0 < 26.5$	130/23	6	145.5	−55.5	9.1	7.2	136.7	5.7	83.4	$5.9 < 7.4 < 26.5$
Mean (N + R)				**22**	**17**	**352.1**	**41.0**	**4.1**	**5.1**	**74.8**	**4.2**	**91.1**	**$3.9 < A_{95\,min}$ (3.8)**		**17**	**335.9**	**54.7**	**7.1**	**5.8**	**63.7**	**4.5**	**39.2**	**$3.9 < 5.8 < 13.8$**

Lat, latitude of the sites; Long, longitude of the site; N, number of samples after interpretation; N_{45}, number of samples application of a fixed cut-off (45°); D, declination; I, inclination; ΔD_x, declination error; ΔI_x, inclination error; k, estimate of the precision parameter determined from the ChRM directions; α_{95}, cone of confidence determined from the ChRM directions; K, precision parameter determined from the mean virtual geomagnetic pole (VGP) direction; A_{95}, cone of confidence determined from the mean VGP direction. $A_{95\,min}$ and $A_{95\,max}$ correspond to the confidence envelope of Deenen et al. (2011). If A_{95} falls within this envelope the distribution likely represents paleosecular variation. If $A_{95} < A_{95\,min}$ the distribution is too tight and represents a spot-reading of the field. All values are given before and after correction for bedding tilt. Strike/dip, bedding planes for the samples included in the calculation of the ChRM directions.

* Site contains both normal and reverse polarity.

4. Paleomagnetic results

Thermomagnetic curves obtained by Curie Balance measurements are shown in Fig. 2. The low magnetization of samples A, D and G suggest that the paramagnetic fraction is predominant. Sample B, E and C confirm the presence of pyrite, which is the most stable, yet not magnetic, iron sulfide. Above 400 °C, pyrite transforms to magnetite during thermal demagnetization (Passier et al., 2001) and it creates spurious NRM direction. Therefore, the NRM direction at high temperatures (above ∼400 °C) is not reliable. The slightly more hyperbolic shape of the heating curves (sample F, H and I) with highest temperature around 580 °C point to the presence of magnetite. The magnetite may occasionally be cation deficient (maghemite) as shown by maximum temperature of ∼620 °C, or a small contribution of hematite (Fig. 2I).

In many samples, a small viscous component is removed at low temperatures (100 °C) or at low alternating fields (∼10 mT). A secondary component with present-day field direction is generally removed at temperatures around 200–240 °C (Fig. 3). Demagnetization analysis supports that in many cases the principal magnetic carrier of the ChRM in samples is carried by magnetite (530–580 °C), although formation of magnetite from pyrite often obscures the results above 400 °C due to spurious magnetizations.

Equal area projections of the ChRM directions of all sites are displayed in Fig. 6. Details per site and locality are given in Fig. 5 and Table 1. The sampled sites can be divided into three main domains: 1) Aksu Basin (AB), 2) Köprüçay Basin (KB) and 3) Manavgat Basin (MB). The magnetic analyses were firstly done on a per site basis, and then the individual directions from sites were combined to obtain mean directions for 8 localities (Fig. 5 and Fig. 6). These are Aksu-North, Aksu-South (both Miocene) and Aksu_Pliocene, Köprüçay-North, Manavgat-Mid and Manavgat-East. The two localities of Köprüçay-South (MN19-21) and Manavgat-West (MN16-18) did not yield reliable results and are not further used (see Fig. 5 and Table 1).

4.1. Aksu Basin (AB)

The results for the Miocene localities from the Aksu Basin (AK-North and AK-South, see Table 1 for details) show coherent directions with small uncertainty (Fig. 6). The locality Aksu-North consists of eight sites and shows both normal and reverse polarities. All normal sites gave good results and their mean direction shows a small scatter before tilt correction ($K = 28.4$, $A_{95} = 2.8$) while it displays a slightly higher scatter after tilt correction ($K = 18$, $A_{95} = 3.5$). On the other hand, the reverse polarity site-mean direction became slightly better clustered after tilt correction ($K = 36.9$, $A_{95} = 6.2$; $K = 43$, $A_{95} = 5.7$). This may be caused by some normal sites still being affected by a present day field overprint which is indistinguishable from the ChRM. We applied the reversal test to the mean direction of the locality before tilt correction, which was negative ($\gamma = 12.7 > \gamma_c = 6.8$). This is primarily caused by the higher inclination of the normal ($I = 52.3°$) versus the reversed ($I = -39.7°$) mean direction. The reversal test was also performed after tilt correction and although it gave a slightly better result, it was still negative, ($\gamma = 10.6 > \gamma_c = 6.8$). The normal polarity site-mean declination (359°) and reversed mean declination (180°) are identical, but the lower inclination of the reversed direction still causes the reversal test to be negative. Nevertheless, it is evident that locality Aksu-North shows no rotation, even if we refer only to the reversed mean direction.

The Miocene results of locality Aksu-South also showed both normal and reversed polarities (Fig. 6). In-situ, normal directions are well clustered (with $D = 002 \pm 5.0$, $K = 31.3$) while the re-

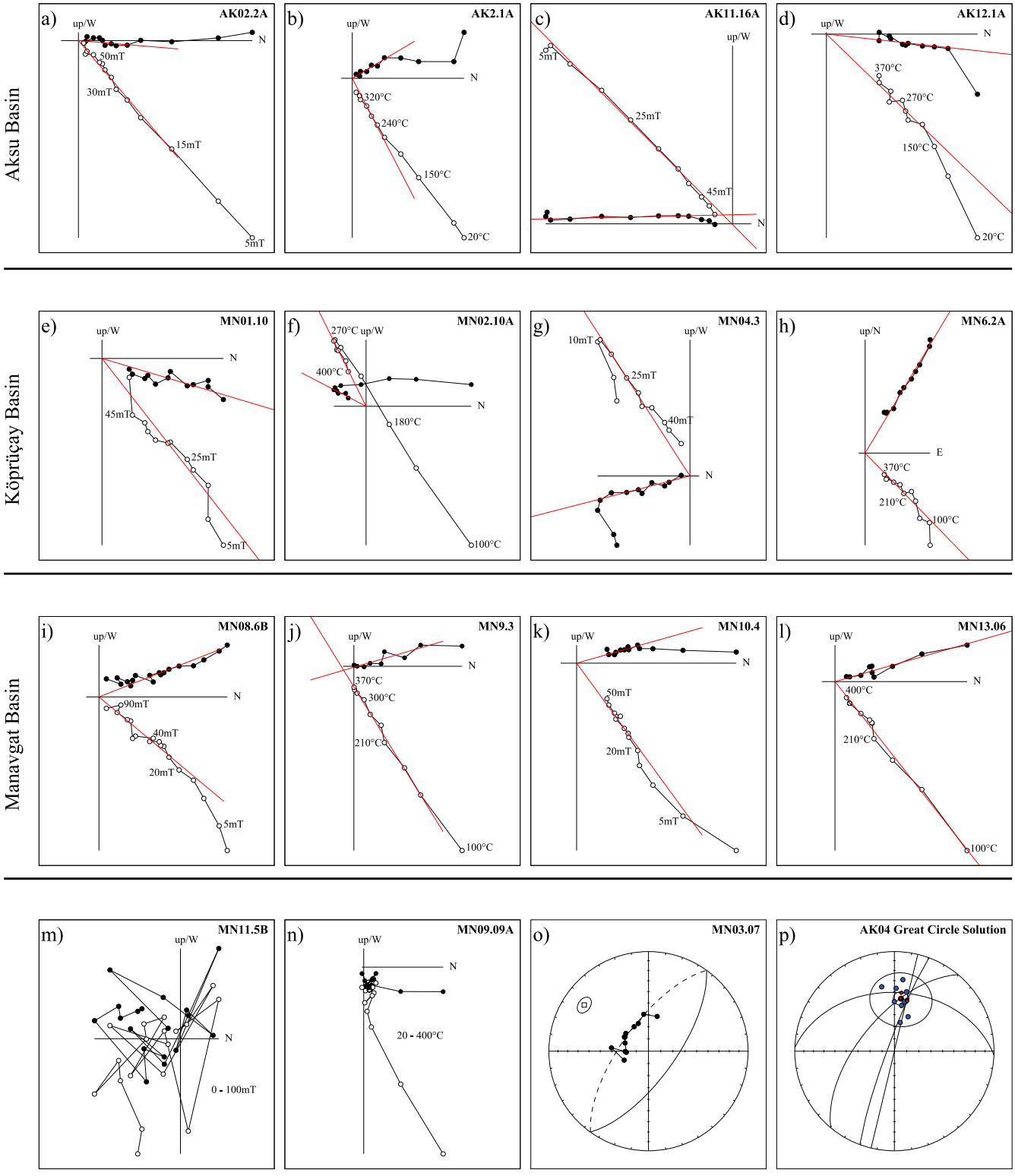

Fig. 3. Orthogonal vector diagrams (Zijderveld, 1967) showing representative demagnetization diagrams for all localities. Closed (open) circles indicate projection on the horizontal (vertical) plane. All diagrams are in a no tilt corrected reference frame. For several samples, both alternating field (steps in milliTesla (mT)) and thermal (steps in °C) demagnetization diagrams are given to show their similarity. For same sites we calculated mean directions according to the method of McFadden and McElhinny (1988).

versed directions are more scattered ($K = 10.3$). After tilt correction, the reversed directions are well clustered ($D = 186° \pm 5.7$, $K = 28.7$), but the normal polarity directions become scattered. For this reason, the normal polarity directions provided a negative fold test, while the reversed directions yielded a positive fold test result (Fig. 6). Hence, the normal polarity samples acquired their NRM after tilting, and likely represent a present-day magnetic field. The inclination of the mean reversed direction ($I = 54.4°$) after 100% unfolding is consistent with the expected geocentric axial dipole field direction at the site latitude (Fig. 6). Hence, we consider the

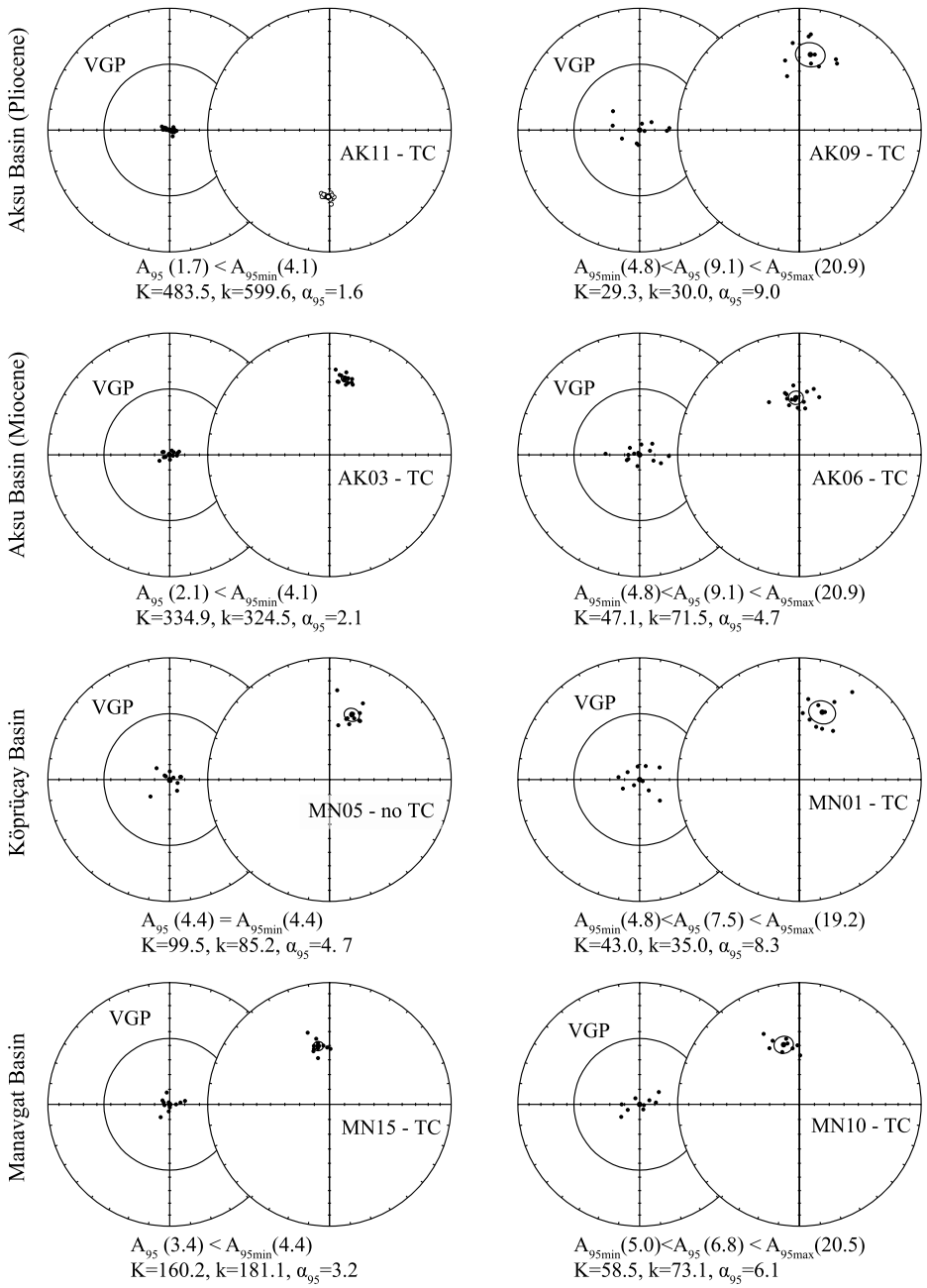

Fig. 4. Examples of the site mean directions according to Deenen et al. (2011) virtual geomagnetic poles (VGP) and their statistical properties were calculated from the ChRM directions.

reversed samples to represent of the primary paleomagnetic direction, and conclude that the Aksu-South region underwent a barely significant vertical axis rotation of $6.0 \pm 5.7°$ since the Early Miocene sediments.

The Aksu Basin has five sites of Pliocene age (Fig. 6), of which 2 have normal and 3 have reversed polarity (Table 1 and Fig. 6). The reversed mean inclination ($-44°$) is slightly lower than the normal mean inclination (50.1°) suggesting that a (recent) overprint has not been fully removed: it causes reversed ChRM direction to be shallower and normal ones to be slightly steeper. It causes the reversal test applied to these site mean directions to be negative ($\gamma = 7.8 > \gamma_c = 6.0$). Both normal and reversed mean directions show no significant vertical rotation since the Pliocene. The mean of the combined normal and reversed data for this locality therefore shows no net rotation (Fig. 6).

4.2. Köprüçay Basin (KB)

The Köprüçay Basin has eight Miocene sites (KB-North, see Table 1 and Fig. 6) with both normal and reversed polarities. Mean directions of normal sites show similar scatter before ($K = 25.1$, $A_{95} = 4.0$) and after tilt correction ($K = 22.6$, $A_{95} = 4.2$). There is also no significant difference between normal mean directions before (012°/42.9°) and after tilt corrections (008°/44.8°), pointing to a small clock-wise vertical rotation. On the other hand, reverse polarity site-mean directions became significantly better clustered ($K = 16.1$, $A_{95} = 8.9$; $K = 40.4$, $A_{95} = 5.5$) after tilt correction. The mean inclination of the reverse site-mean before tilt correction is steep ($I = 59.1°$), more than the expected geocentric axial dipole field direction at the site latitude ($I = 56°$). After tilt correction, the mean inclination is more realistic ($I = -44°$) lower than the

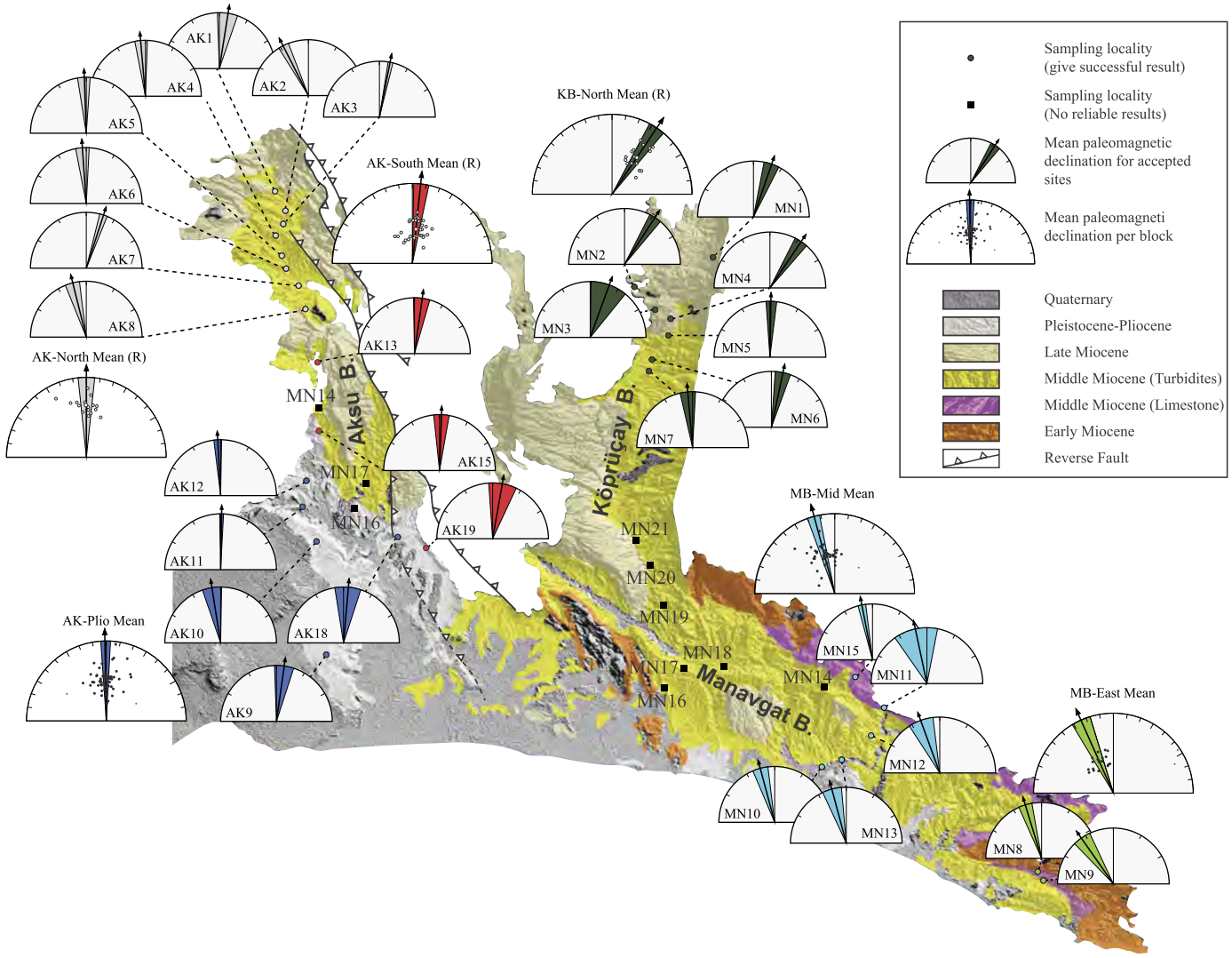

Fig. 5. Map shows locations of the sites and declinations with their corresponding ΔD_x (colored shading) for this study. The same color indicates each sub-area combined from the individual directions from sites.

expected geocentric axial dipole inclination ($I = 56.4°$) due to inclination shallowing.

The reversal test applied to in-situ data is negative ($\gamma = 16.4 > \gamma_c = 9.5$). The normal mean direction differs from the reversed mean direction, in particular because of the different inclinations of the normal (42.9°) and reversed (59.1°) sites. The reversal test was also performed after tilt correction and it was again negative ($\gamma = 18.4 > \gamma_c = 6.7$), showing that normal and reverse polarity data are not antipodally distributed. This time, however, there is no large difference between the mean normal and reversed inclinations, but the reversed mean direction (214°/−44) is significantly different from the normal mean direction (008°/44.8°) after tilt correction. We can only explain this by assuming that the normal polarity directions were produced from a mixture of the present-day magnetic field and the primary paleomagnetic direction. Additionally, we applied a fold test to both normal and reversed polarity directions and it indicates an optimal clustering at ∼40% of untilting. When we applied the fold test to only the reversed directions, the best clustering of the paleomagnetic data occurs at 80% unfolding (given in supplementary data) and within error we consider this fold test as positive. Given the widespread evidence for large-scale slumping, followed by folding, we suggest that the first phase of folding (e.g., Çiner et al., 2008) likely reflects soft-sediment deformation prior to acquisition of the magnetization, and that the second phase represents tectonic deformation. If we consider the reversed samples as more reliable and indicative of the primary paleomagnetic direction, the Köprüçay Basin underwent vertical axis rotation of $33 \pm 5.5°$ since the Early Miocene. Alternatively, we may suggest a conservative average of normal and reversed pointing to ∼20° clockwise vertical rotation.

From the southern part of the Köprüçay Basin, KB-South (MN19, 20 and 21 in Table 1 and Fig. 5), we did not record reliable data. Results from Site MN19 shows only a normal polarity direction clustered around the geocentric axial dipole field direction before tilt correction. After tilt correction, the directions are scattered and hence the normal polarity samples acquired their NRM after tilting, and thus the signal likely represents a present-day magnetic field. Site 20 and 21 both show reversed polarity, but only great circle solutions are possible without any set points. This does not create a reliable result for determining vertical axis rotations.

In summary, we find a minimum of ∼20° CW rotation in Köprüçay Basin since the Middle Miocene. However, we consider the ∼33° clockwise (CW) rotation shown by the reversed polarity data most reliable because they cannot have been mixed with present-day field normal overprinted directions.

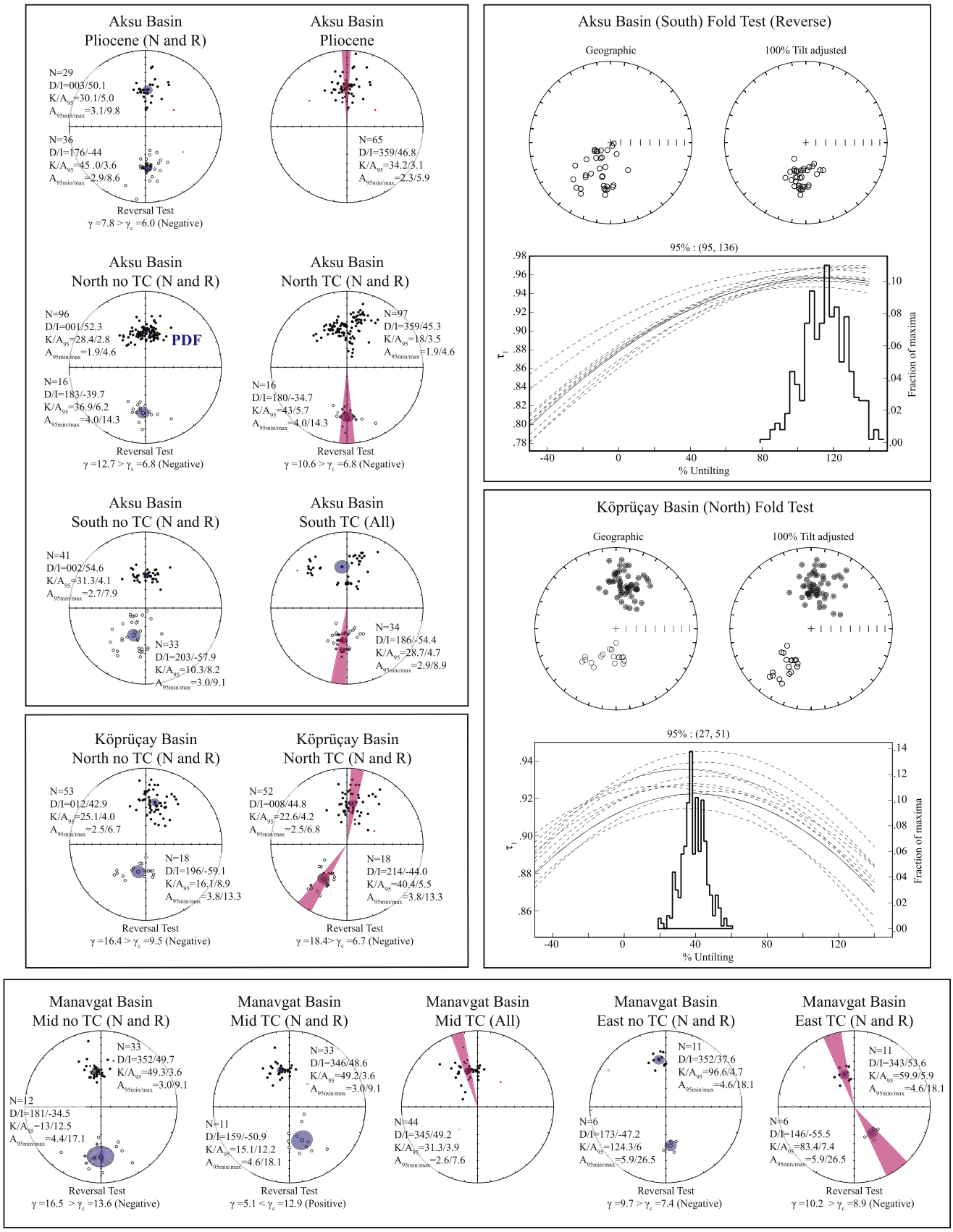

Fig. 6. Equal area projection of the ChRM directions for Aksu, Köprüçay and Manavgat Basins. Closed (open) symbols indicate projection on lower (upper) hemisphere. Large black symbols with blue transparent circle denote respectively the mean directions and their cone of confidence (α_{95}). Red small circles indicate the individual directions rejected after application of fixed 45° cut-off. Reversals test results were calculated by the method of McFadden and McElhinny (1990). Fold test of Tauxe and Watson (1994) for Aksu and Köprüçay Basins. (For interpretation of the references to color in this figure legend, the reader is referred to the web version of this article.)

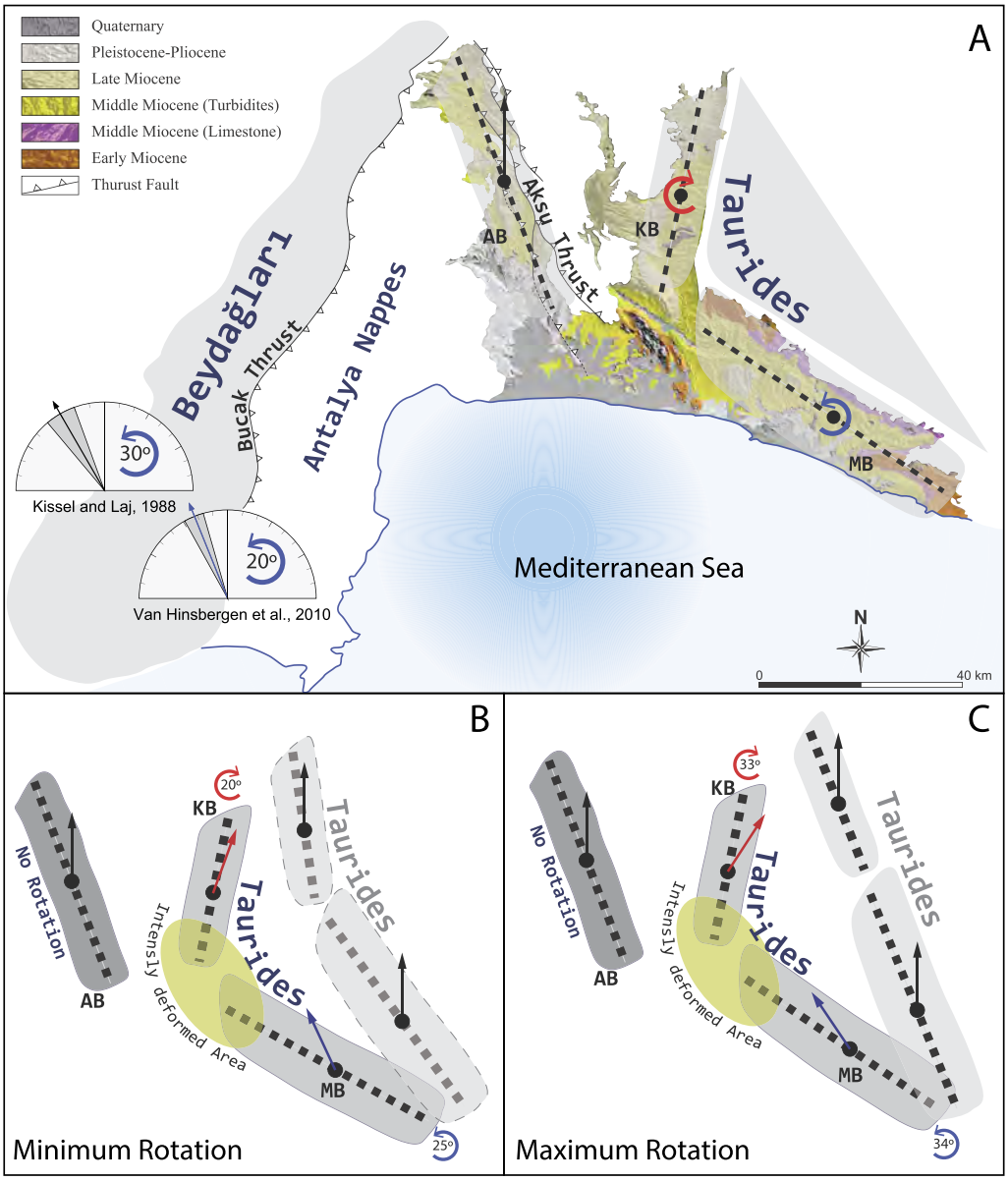

Fig. 7. (A) Overview of all declinations and their error envelope per locality indicated on the regional geological map of the study area. (B and C) Possible restoration scenario of the Miocene marine sediments and Taurides based on their minimum and maximum rotations: Highlighted blocks are present-day configuration of the Miocene Basins. Gray domains represent areas covered by the Miocene marine sediments, dark dash lines show the orientation of the long axis of the basin formation. Yellow circle area indicates highly deformed areas due to bending of the Taurides (there are no significant rotation results). Transparent areas indicate possible geologic configuration of the basins and the Taurides before rotation event. Blue arrows indicate counter-clockwise rotation (CCW). Red arrows show clockwise rotation (CW). Black arrows represent the present-day geographic north direction. AB: Aksu Basin, KB: Köprüçay Basin and MB: Manavgat Basin. (For interpretation of the references to color in this figure legend, the reader is referred to the web version of this article.)

4.3. Manavgat Basin (MB)

The results for the Miocene localities from the Manavgat Basin are divided into three localities (see Table 1 and Fig. 6 for details) of which two (MB-Mid and MB-East) show coherent directions. Similar to KB-South, MB-West (MN16, 17 and 18) did not give reliable results. Both localities are in the intensely deformed area (Fig. 7). Site MN16 shows reversed directions; for this site only great circle solutions are possible, but without any set points. Site MN17 and MN18 represent normal directions and are highly scattered in-situ while after tilt correction the inclination of these sites is extremely steep.

The locality MB-Mid consists of six sites. One of them (MN14) did not yield reliable results, because before tilt correction it corresponds to the present-day magnetic field, whereas after tilt correction, the inclination of this site is too steep for a primary ChRM direction. The locality shows both normal and reversed polarities. Mean directions of normal sites show the same statistical properties before ($K = 49.3$, $A_{95} = 3.6$) and after ($K = 49.2$, $A_{95} = 3.6$) tilt correction. On the other hand, reversed polarity site-mean directions show higher scatter, both before ($K = 13.0$, $A_{95} = 12.5$) after tilt correction ($K = 15.1$, $A_{95} = 12.2$). A reversal test was applied to the in-situ data, which was negative ($\gamma = 16.5 > \gamma_c = 13.6$) mainly due to the large difference in inclination. The mean declination of the reversed site-mean before tilt correction is much shallower ($I = -34.5°$) than the inclination of normal mean ($I = 49.7°$). However, the reversal test performed after tilt correction is positive ($\gamma = 5.1 < \gamma_c = 12.9$, classification C) pointing to reliable pre-tilt directions for both polarities. Typically, inclinations are shallower (by $>10°$) due to compaction and in-

clination shallowing. Additionally, we applied a fold test to both normal and reversed polarity and it indicates an optimal clustering at ~80% of untilting (given in supplementary data), with large uncertainties (95% confidence level, untilting between 41 and 98%), but we consider it is positive because the reversal test is also positive. The result of the five sites on average shows a robust counter-clockwise vertical rotation of 15° ± 4.5 since the Late Miocene.

The locality MN-East consists of two Middle Miocene sites, one is normal (MN8) and one is reversed (MN9). The normal site gave good results and its mean directions with a small scatter ($K = 96.6$, $A_{95} = 4.7$) is well clustered at 352 ± 5.0, but its mean inclination ($I = 37.6°$) is quite low with respect to the expected inclination at the site latitude before tilt correction. Similarly, the mean of the reversed site is also well clustered at 173 ± 6.9, also with a small scatter ($K = 124.3$, $A_{95} = 6.0$), which is very close to declination of normal site, but the inclination ($I = 47.2°$) is significantly different from the normal site by 10°. This caused the reversal test before tilt correction to be negative ($\gamma = 9.7 > \gamma_c = 7.4$). After tilt correction, normal directions are slightly more scattered ($K = 59.9$, $A_{95} = 5.9$), but still well clustered at 343° ± 7.2. Reversed directions are also well clustered at 146 ± 9.1 with a small scatter ($K = 83.4$, $A_{95} = 7.4$). The tilt correction causes the inclinations to be very similar ($I = 53.6°$ and $I = 55.5°$, respectively). The reversal test after tilt correction was also negative ($\gamma = 10.2 > \gamma_c = 8.9$), because now the mean declinations of the normal and reversed sites are significantly different. Likely, we have not sufficiently removed a present-day field overprint. To average out its influence on normal and reverse direction, we conclude that a conservative average of normal and reverse points to a ~25° counter-clockwise (CCW) vertical rotation. The mean direction of the normal and reverse data from this locality provides clear evidence that the Manavgat Basin underwent a net counter-clockwise rotation of 25 ± 8.1°. If we consider the reversed samples as indicative of the primary paleomagnetic direction, the Manavgat Basin was subjected to a counter-clockwise vertical axis rotation of 34 ± 9.1° since the Middle Miocene.

5. Discussion

5.1. Orocline formation and restoration

Our new paleomagnetic results of basins within the Isparta Angle show that each basin recorded different and independent rotations, and they can be considered paleomagnetically coherent structural entities since the Early Miocene. The Aksu Basin has undergone only very minor rotations during and after the Miocene, consistent with previous results of Kissel and Poisson (1986). The paleomagnetic data from Köprüçay and Manavgat basins show 20–30° clockwise and counter-clockwise rotation, respectively. The rotation angle between these basins appears to be proportional to the strikes of their modern eastern basin margins and general strike of its tilted beds. The orocline test (Schwartz and Van der Voo, 1983; Eldredge et al., 1985) (Fig. 8) was carried out based on the paleomagnetic directions from the Miocene. Local structural directions derived from local bedding strike (Table 1) and regional fold axis directions obtained from geological maps (1/100.000 scale) produced by the General Directorate of Mineral Research and Exploration (MTA). The result of the test yields a slope of the regression line of $m = 0.56 \pm 0.16$; between $m = 1$ (100% positive orocline test) and $m = 0$ (negative orocline test). This slope and its error suggests that on average some 50–70% of the curvature of the Central Taurides was acquired by the end of the Miocene, while the remaining 30–50% of the curvature was acquired after the Miocene. In Fig. 7, we use the observed rotation pattern and give a possible restoration by back-rotation of the Köprüçay and Manavgat basins. The restored configuration shows that the two

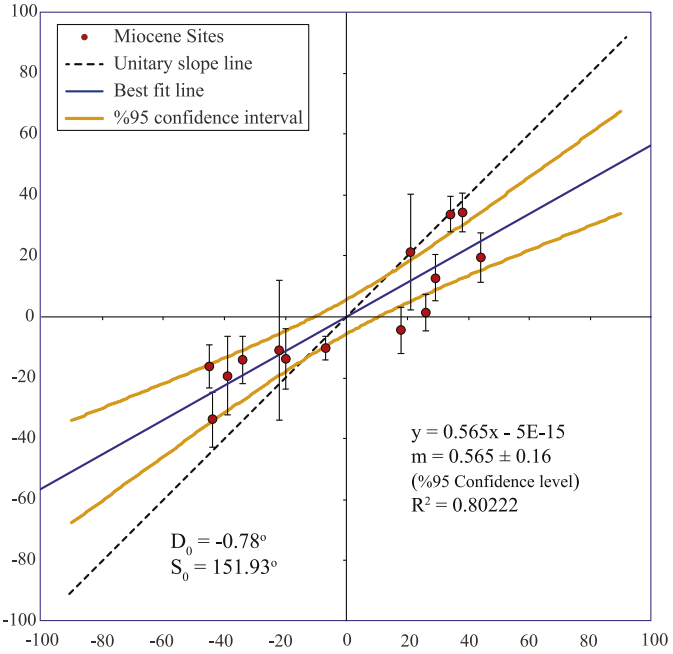

Fig. 8. Paleomagnetic declination deviations for 14 Miocene sites (after tilt correction) relative to strike of the orocline. D is the observed paleomagnetic declination at a site, and D_0 is the mean (reference) declination value. S is the observed orocline strike (obtained from bed measurement or fold axis). S_0 is the mean (reference) strike of the orocline. Error bars for declination data and α_{95} confidence level of the regression line are also given in the graph.

basins were largely collinear in ~N(NW) direction, and essentially parallel to the orientation of Aksu Basin. This structural configuration may indicate that the Aksu, Köprüçay and Manavgat basins developed on top of moving thrust sheets as piggy-back basins, as a part of a larger foreland basin system at the western front of the Central Tauride fold-thrust belt. Subsequent oroclinal bending reflected by the vertical axis rotations shows that horizontal displacements vary laterally and are maximum at the intersection of the Köprüçay and Manavgat basins (Fig. 7).

Our results shed a new light on the kinematic evolution of the junction between the Aegean and Cyprus arcs. Previous paleomagnetic studies showed that the Beydağları platform and the Lycian nappes in the western limb of the Isparta Angle underwent ~20–30° post-Early Miocene CCW rotation (Kissel and Poisson, 1987; Kissel and Laj, 1988; van Hinsbergen et al., 2010a). Van Hinsbergen et al. (2010a) and van Hinsbergen (2010) proposed a scenario in which the counterclockwise rotating Beydağları block was bounded in the east by the Aksu thrust and the Kırkkavak fault, widely presumed to have a strike-slip component that would partition right-lateral transpression. That scenario implied that the Aksu Basin was part of the rotating domain of Beydağları. Our new data convincingly demonstrate that this cannot be the case, however, and therefore we need to re-evaluate the kinematic history of the region.

First, van Hinsbergen et al. (2010a) concluded that the rotation of Beydağları should have ended before the Pliocene (5 Ma), based on paleomagnetic results of Kissel and Poisson (1986) from the Aksu Basin. We now show that the Aksu Basin was not part of the same tectonic domain as the Beydağları platform, and the rotation of Beydağları may thus have continued into the Pliocene. Second, the rotation of Beydağları cannot have been bounded by the Aksu thrust, but must be bounded by a structure to the west of the Aksu basin. The most likely candidate for this structure is the Bucak thrust, which emplaced Mesozoic limestones and overlying Antalya nappes that constitute the basement of the Aksu Basin over Miocene and older sediments of Beydağları (Fig. 9). Farther

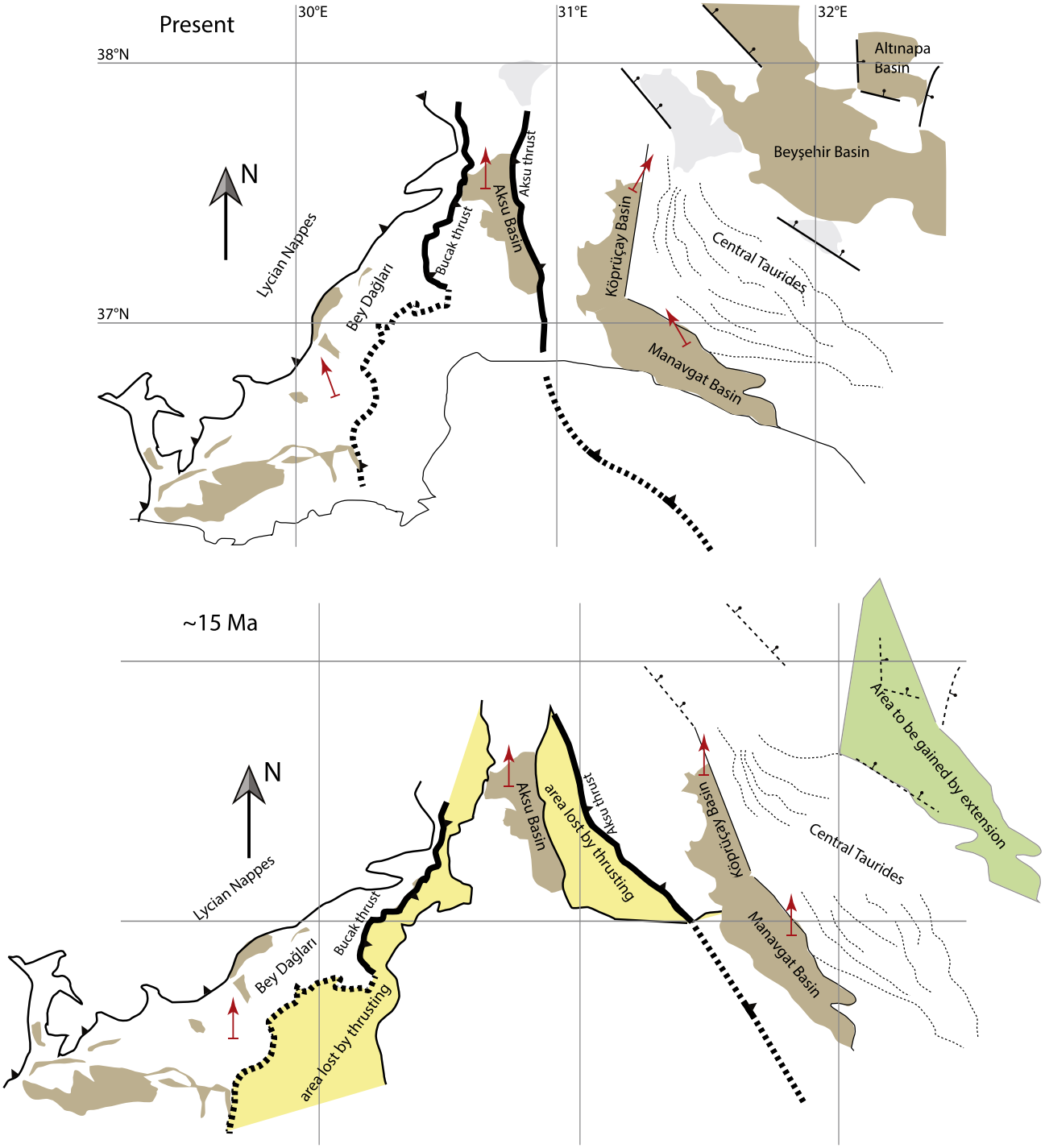

Fig. 9. Present-day (top panel) and middle Miocene (bottom panel) basin and thrust configurations in SW Anatolia based on the paleomagnetic results collected in our study.

to the south, the Antalya Nappes thrust over Miocene sediments that cover Beydağları (Hayward and Robertson, 1982). We tentatively suggest that the Bucak Thrust may connect southward to this structure (Fig. 9), and accommodated a total Miocene displacement of several tens of kilometers. In addition, we can conclude that also the Aksu thrust must have played a significant role, but now in accommodating 20–30° vertical axis rotation difference between the Köprüçay and Aksu basins together with up to tens of kilometers of convergence.

Whereas the Miocene oroclinal bending in the heart of the Isparta Angle is accompanied by E–W shortening, resulting in area loss, to the east it is accompanied by area gain due to extension (Fig. 9). Koç et al. (2012, 2015) showed that the Altınapa and Yalvaç basins, restricted continental basins located approximately 100 km N and NE of the study area, are extensional basins. This extension remains active today and started at least during the middle Miocene, and was multi-directional in nature. Where the N–S component of extension may be explained by some southward retreat of the Cyprus slab relative to Anatolia (Flecker et al., 2005), the E–W component of the extension that formed most of the range-bounding structures may be kinematically linked to the oroclinal bending constrained here.

From Early-Middle Miocene to at least Pliocene times, E–W shortening along the Aksu thrust (Poisson et al., 2003; Çiner et al., 2008) and likely along the Bucak thrust in the Isparta Angle is puzzling in the context of the N–S plate convergence between Africa

and Eurasia. Similarly, Hall et al. (2014) documented offshore continuation of this N–S striking thrust system in the Bay of Antalya. Given the widespread evidence for westward escape of Anatolia relative to Eurasia and Arabia, previous authors have suggested a kinematic link between the Aksu Thrust and westward Anatolian escape (Şengör and Yılmaz, 1981; Glover and Robertson, 1998; Poisson et al., 2003; Deynoux et al., 2005; Hall et al., 2014). As recently pointed out by Koç et al. (2015), the E–W extension component in the eastern limb of the Isparta Angle, as well as the E–W to NE-SW extension in central Anatolia (Koçyiğit and Özacar, 2003) makes a connection to push from the east unlikely.

Koç et al. (2015) recently connected the contemporaneous E–W shortening in the center and the E–W extension component in the eastern limb of the Isparta Angle to previously published seismological observations from the mantle underlying the Central Taurides. Seismic tomographic images of Biryol et al. (2011) (Fig. 1d), and a study focused on earthquake hypocenters in the mantle below the study area (Kalyoncuoğlu et al., 2011) have shown that there are two separate slab segments below southern Turkey: 1) the Cyprus slab, a northwards dipping slab below Cyprus, which in most of the upper mantle can be tomographically discerned from 2) the Antalya slab (*sensu* Koç et al., 2015), an eastwards dipping, N–S striking slab with an associated Benioff zone under the Central Taurides,. This Antalya slab (Fig. 1d) is clearly separated from the Aegean slab along a transform fault (STEP fault, *sensu* Govers and Wortel, 2005) as shown in seismic tomographic images of van Hinsbergen et al. (2010c), and Biryol et al. (2011). Westward retreat of this subduction zone relative to Central Anatolia would give way to simultaneous contraction (in the fore-arc region in the west) and extension (towards the back-arc region in the east) within the overriding plate. Seismicity patterns, geological studies, and seismic profiles (e.g., Hall et al., 2014) have so far not shown that E–W contraction is still active today and that the Antalya slab has no known connection to the surface. If the slab has entirely broken off, it must have done so recently so as to still generate a Benioff zone, and not generate a visible gap in the tomography. We propound that it was the lateral propagation of break-off of the Antalya slab *sensu* Wortel and Spakman (2000) that focused its surface expression on an increasingly narrow region experiencing trench retreat relative to Central Anatolia, with the Miocene oroclinal bending documented in this paper as a result.

Our study highlights that the subduction zone configuration consuming the African plate below Anatolia until times as young as the Quaternary or even today, may have been more complex than generally assumed. The modern subducted lithosphere configuration has been accurately portrayed by seismic tomographic images (Fig. 1d) (Biryol et al., 2011), and segmentation of the subducting plate into separate slabs may have lead to strong regional variations in tectonic history and styles, including the progressive orocline formation documented in this study. Several authors (Deynoux et al., 2005; Cosentino et al., 2012; Schildgen et al., 2012a, 2012b, 2014) have recently explored the effects that separate slabs below SW Anatolia may have had on asthenospheric flow between the slabs and possible dynamic topographic effects. In addition to these studies, our study indicates that the deformation history, and perhaps even active tectonics, may be strongly affected by these complex slab configurations. Our study further provides evidence that E–W shortening in the heart of the Isparta Angle is a subduction-driven process and not a local space problem associated with Anatolian escape. Since the subducting Antalya slab still has a Benioff zone (Kalyoncuoğlu et al., 2011) and the overriding plate undergoes active extension (Koç et al., 2012, 2015), we highlight the urge to study the heart of the Isparta Angle for recent and active tectonics, e.g. through tectonic geomorphology and GPS campaigns, to assess whether the area poses an underappreciated seismic hazard.

6. Conclusions

In this paper, we provide a paleomagnetic study of Miocene marine sediments in the heart of the Isparta Angle in southwest Turkey, to evaluate to what extent vertical axis rotations accompanied well-documented Neogene contraction. Our main findings can be summarized as follows:

Three different rotational domains are distinguished east of the Beydağları platform that was previously shown to have rotated 20° CCW: (1) The Köprüçay Basin in the north recorded ∼20–30° CW rotation, (2) the Manavgat Basin in the south shows ∼25–35° CCW rotation and (3) the Aksu Basin in the west shows no significant rotation since at least Middle Miocene. The restored original configurations of Köprüçay and Manavgat basins show that they were essentially aligned in ∼N(NW) direction at an early stage of their history, and parallel to the orientation of the Aksu basin.

The rotation domains are separated by major thrust faults that may have accommodated some tens of kilometers of Miocene contraction. The rotation of Beydağları relative to the Aksu Basin was likely accommodated along the Bucak Thrust. The rotation of the Köprüçay relative to the Aksu basin was accommodated along the Aksu thrust. In addition, oroclinal bending was likely accommodated in the east by the E–W dominated multidirectional extension documented previously (Koç et al., 2012, 2015) in the east of the Central Taurides.

We explain oroclinal bending in the context of a recently realized complex subduction zone configuration of SW Turkey. Koç et al. (2015) recently explained contemporaneous E–W shortening in the heart of the Isparta Angle and multidirectional extension in the eastern limb of the Isparta Angle to result from westward retreat of a narrow, ∼N–S trending Antalya slab below the Isparta Angle. This slab, which still has a Benioff zone and is well imaged by tomography, has no known active surface connection, which may indicate that it has very recently broken off. The westward retreat of the Antalya slab during lateral propagation of break-off would focus its surface expression to an increasingly narrow zone, which could explain oroclinal bending. The Bucak thrust may form the most recent surface connection of the Antalya slab.

Recent studies explored how a complex slab configuration of the subducting African plate may affect asthenospheric upwelling and dynamic topography. Our study highlights that the Neogene deformation history, and perhaps even active tectonics, may be strongly affected by these complex slab configurations in SW Turkey.

Acknowledgements

Daniel Pastor Galan's help with the orocline test elements of this paper is greatly appreciated. Iuliana Vasiliev is thanked for her very constructive contribution on interpretation of Curie Balance data. Research for this paper occurred within the context of the Netherlands Research School of Integrated Solid Earth Sciences (ISES) and was supported by ÖYP research fund of Turkish Government (No: BAP-08-11-DPT.2002K120510), TÜBİTAK (the Scientific and Technological Research Council of Turkey) International Postdoctoral Research Fellowship Programme (2219), TÜBİTAK project Grant number (ÇAYDAG-111Y239) and the DARIUS programme. D.J.J.v.H. acknowledges ERC Starting Grant number 306810 (SINK) and NWO VIDI grant 864.11.004. Murat Özkaptan, Kıvanç Yücel and Pınar Ertepınar are acknowledged for their help during fieldworks in 2010 and 2013. We thank Rob Van der Voo and an anonymous reviewer for valuable comments.

Appendix A. Supplementary material

Supplementary material related to this article can be found online at http://dx.doi.org/10.1016/j.epsl.2015.11.020.

References

Andrew, T., Robertson, A.H., 2002. The Beyşehir–Hoyran–Hadim Nappes: genesis and emplacement of Mesozoic marginal and oceanic units of the northern Neotethys in southern Turkey. J. Geol. Soc. 159, 529–543.

Biryol, C.B., Beck, S.L., Zandt, G., Özacar, A.A., 2011. Segmented African lithosphere beneath the Anatolian region inferred from teleseismic P-wave tomography. Geophys. J. Int. 184, 1037–1057.

Blumenthal, M.M., 1963. Le système structural du Taurus sud Anatolies. Bull. Soc. Géol. Fr. (Livre à Mémoire de Professor P. Fallot, Mémoir hors-série) 1, 611–662.

Butler, R.F., 1992. Paleomagnetism: Magnetic Domains to Geologic Terranes. Blackwell Publishing, Boston. 195 p.

Collins, A.S., Robertson, A.H.F., 2003. Kinematic evidence for Late Mesozoic–Miocene emplacement of the Lycian Allochthon over the Western Anatolide Belt, SW Turkey. Geol. J. 38, 295–310.

Cosentino, D., Schildgen, T.F., Cipollari, P., Faranda, C., Gliozzi, E., Hudackova, N., Lucifora, S., Strecker, M.R., 2012. Late Miocene surface uplift of the southern margin of the Central Anatolian Plateau, Central Taurides, Turkey. Geol. Soc. Am. Bull. 124, 133–145.

Çiner, A., Karabıyıkoğlu, M., Monod, O., Deynoux, M., Tuzcu, S., 2008. Late Cenozoic sedimentary evolution of the Antalya Basin, Southern Turkey. Turk. J. Earth Sci. 17, 1–41.

Deenen, M.H.L., Langereis, C.G., van Hinsbergen, D.J.J., Biggin, A.J., 2011. Geomagnetic secular variation and the statistics of palaeomagnetic directions. Geophys. J. Int. 186, 509–520.

Deynoux, M., Çiner, A., Karabıyıkoğlu, M., Monod, O., Manatschal, G., Tuzcu, S., 2005. Facies architecture and depositional evolution of alluvial fan to fan-delta complexes in the tectonically active Miocene Köprüçay Basin, Isparta Angle, Turkey. Sediment. Geol. 173, 289–317.

Eldredge, S., Bachtadse, V., Van der Voo, R., 1985. Paleomagnetism and the orocline hypothesis. Tectonophysics 119, 153–179.

Ergin, M., Aktar, M., Özalaybey, S., Tapirdamaz, M.C., Selvi, O., Tarancıoglu, A., 2009. A high-resolution aftershock seismicity image of the 2002 Sultandağı-Çay earthquake (Mw = 6.2), Turkey. J. Seismol. 13, 633–646.

Faccenna, C., Bellier, O., Martinod, J., Piromallo, C., Regard, V., 2006. Slab detachment beneath eastern Anatolia: a possible cause for the formation of the North Anatolian fault. Earth Planet. Sci. Lett. 242, 85–97.

Flecker, R., Poisson, A., Robertson, A.H.F., 2005. Facies and palaeogeographic evidence for the Miocene evolution of the Isparta Angle in its regional eastern Mediterranean context. In: Kelling, G., Robertson, A.H.F., Vanbuchen, F. (Eds.), Cenozoic Sedimentary Basins of South Central Turkey. Sediment. Geol. 173, 277–314.

Glover, C., Robertson, A.H.F., 1998. Neogene intersection of the Aegean and Cyprus arcs: extensional and strike-slip faulting in the Isparta Angle, SW Turkey. Tectonophysics 298, 103–132.

Govers, R., Wortel, M.J.R., 2005. Lithosphere tearing at STEP faults: response to edges of subduction zones. Earth Planet. Sci. Lett. 236, 505–523.

Hall, J., Aksu, A.E., King, H., Gogacz, A., Yaltırak, C., Çifçi, G., 2014. Miocene – recent evolution of the western Antalya Basin and its linkage with the Isparta Angle, eastern Mediterranean. Mar. Geol. 349, 1–23.

Hayward, A.B., 1984. Miocene clastic sedimentation related to the emplacement of the Lycian Nappes and the Antalya Complex, SW Turkey. Geol. Soc. (Lond.) Spec. Publ. 17, 287–300.

Hayward, A.B., Robertson, A., 1982. Direction of ophiolite emplacement inferred from Cretaceous and Tertiary sediments of an adjacent autochthon, the Bey Dağları, southwest Turkey. Geol. Soc. Am. Bull. 93, 68–75.

Hüsing, S.K., Zachariasse, W.J., van Hinsbergen, D.J.J., Krijgsman, W., Inceöz, M., Harzhauser, M., Mandic, O., Kroh, A., 2009. Oligo-Miocene basin evolution in SE Anatolia: constraints on the closure of the eastern Tethys gateway. In: van Hinsbergen, D.J.J., Edwards, M.A., Govers, R. (Eds.), Collision and Collapse at the Africa–Arabia–Eurasia Subduction Zone. In: Geol. Soc. Lond. Spec. Publ., vol. 311, pp. 107–132.

Kalyoncuoğlu, Ü.Y., Elitok, Ö., Dolmaz, M.N., Anadolu, N.C., 2011. Geophysical and geological imprints of southern Neotethyan subduction between Cyprus and the Isparta Angle, SW Turkey. J. Geodyn. 52 (1), 70–82.

Karabıyıkoğlu, M., Tuzcu, S., Çiner, A., Deynoux, M., Örçen, S., Hakyemez, A., 2005. Facies and environmental setting of the Miocene coral reefs in the late-orogenic fill of the Antalya Basin, western Taurides, Turkey: implications for tectonic control and sea-level changes. Sediment. Geol. 173, 345–371.

Kirschvink, J.L., 1980. The least-square line and plane and the analysis of paleomagnetic data. Geophys. J. R. Astron. Soc. 62, 699–718.

Kissel, C., Poisson, A., 1986. Etude paléomagnétique préliminaire des formations néogènes du bassin d'Antalya (Taurides occidentales, Turquie). C. R. Acad. Sci. Paris 302, 711–716.

Kissel, C., Poisson, A., 1987. Étude paléomagnetique préliminaire des formations cénozoïques des Bey Dağları (Taurides occidentales, Turquie). C. R. Acad. Sci., Sér. 2 304, 343–348.

Kissel, C., Laj, C., 1988. The tertiary geodynamical evolution of the Aegean arc: a paleomagnetic reconstruction. Tectonophysics 146, 183–201.

Kissel, C., Averbuch, O., Frizon de Lamotte, D., Monod, O., Allerton, S., 1993. First paleomagnetic evidence for a post-Eocene clockwise rotation of the Western Taurides thrust belt east of the Isparta reentrant (Southwestern Turkey). Earth Planet. Sci. Lett. 117, 1–14.

Koç, A., Kaymakci, N., van Hinsbergen, D.J.J., Kuiper, K.F., Vissers, R.L.M., 2012. Tectono-sedimentary evolution and geochronology of the Middle Miocene Altınapa Basin, and implications for the Late Cenozoic uplift history of the Taurides, southern Turkey. Tectonophysics 532–535, 134–155.

Koç, A., Kaymakci, N., van Hinsbergen, D.J.J., Vissers, R.L.M., 2015. A Miocene onset of the modern extensional regime in the Isparta Angle: constraints from the Yalvaç Basin (southwest Turkey). Int. J. Earth Sci. (Geol. Rundsch.). http://dx.doi.org/10.1007/s00531-014-1100-z (in press).

Koçyiğit, A., Özacar, A.A., 2003. Extensional Neotectonic regime through the NE edge of the outer Isparta Angle, SW Turkey: new field and seismic data. Turk. J. Earth Sci. 12, 67–90.

Koçyiğit, A., Ünay, E., Saraç, G., 2000. Episodic graben formation and extensional neotectonic regime in west Central Anatolia and the Isparta Angle: a case study in the Akşehir-Afyon Graben, Turkey. In: Bozkurt, E., Winchester, J.A., Piper, J.D.A. (Eds.), Tectonics and Magmatism in Turkey and the Surrounding Area. In: Geol. Soc. (Lond.) Spec. Publ., vol. 173, pp. 405–421.

McFadden, P.L., McElhinny, L.W., 1988. The combined analysis of remagnetization circles and direct observations in palaeomagnetism. Earth Planet. Sci. Lett. 87, 161–172.

McFadden, P.L., McElhinny, M.W., 1990. Classification of the reversal test in paleomagnetism. Geophys. J. Int. 103, 725–729.

Meijers, M.J.M., van Hinsbergen, D.J.J., Dekkers, M.J., Altıner, D., Kaymakcı, N., Langereis, C.G., 2011. Pervasive Paleogene remagnetization of the central Taurides fold-and-thrust belt (southern Turkey) and implications for rotations in the Isparta Angle. Geophys. J. Int. 184, 1090–1112.

Morris, A., Robertson, A.H.F., 1993. Miocene remagnetisation of carbonate platform and Antalya Complex units within the Isparta Angle, SW Turkey. Tectonophysics 220, 243–266.

Mullender, T.A.T., van Velzen, A.J., Dekkers, M.J., 1993. Continuous drift correction and separate identification of ferromagnetic and paramagnetic contribution in thermomagnetic runs. Geophys. J. Int. 114, 663–672.

Okay, A.I., 1989. Geology of the Menderes Massif and the Lycian Nappes south of Denizli, western Taurides. Miner. Resour. Explor. Bull. 109, 37–51.

Okay, A.I., Zattin, M., Cavazza, W., 2010. Apatite fission-track data for Miocene Arabia–Eurasia collision. Geology 38, 35–38.

Özgül, N., 1976. Some geological aspects of the Taurus orogenic belt (Turkey). Bull. Geol. Soc. Turk. 19, 65–78 (in Turkish).

Özgül, N., 1984. Stratigraphy and tectonic evolution of the central Taurus. In: Tekeli, O., Göncüoğlu, M.C. (Eds.), Geology of the Taurus Belt. MTA, Ankara, pp. 77–90.

Passier, H.F., de Lange, G.J., Dekkers, M.J., 2001. Rock-magnetic properties and geochemistry of the active oxidation front and the youngest sapropel in the Mediterranean. Geophys. J. Int. 145, 604–614.

Poisson, A., Wernli, R., Sagular, E.K., Temiz, H., 2003. New data concerning the age of the Aksu Thrust in the south of the Aksu valley, Isparta Angle (SW Turkey): consequences for the Antalya Basin and the Eastern Mediterranean. Geol. J. 38, 311–327.

Poyraz, S.A., Pınar, A., Özden, S., Tunçer, M.K., 2014. Implications of 2007's earthquake activity in Eğirdir Lake (SW Anatolia) based on moment tensor solutions and inversion of stress state. Pure Appl. Geophys. 171, 1299–1309. http://dx.doi.org/10.1007/s00024-013-0715-5.

Reilinger, R., McClusky, S., Vernant, P., et al., 2006. GPS constraints on continental deformation in the Africa–Arabia–Eurasia continental collision zone and implications for the dynamics of plate interactions. J. Geophys. Res. 111, BO5411.

Reilinger, R., McClusky, S., Paradissis, D., Ergintav, S., Vernant, P., 2010. Geodetic constraints on the tectonic evolution of the Aegean region and strain accumulation along the Hellenic subduction zone. Tectonophysics 488, 22–30.

Robertson, A.H.F., Woodcock, N.H., 1982. Sedimentary history of the southwestern segment of the Mesozoic–Tertiary Antalya continental margin, southwest Turkey. Eclogae Geol. Helv. 75, 517–562.

Robertson, A.H.F., Poisson, A., Akıncı, Ö., 2003. Developments in research concerning Mesozoic–Tertiary Tethys and neotectonics in the Isparta Angle, SW Turkey. Geol. J. 38, 195–234.

Schildgen, T.F., Cosentino, D., Caruso, A., Buchwaldt, R., Yıldırım, C., Bowring, S.A., Rojay, B., Echtler, H., Strecker, M.R., 2012a. Surface expression of Eastern Mediterranean slab dynamics: neogene topographic and structural evolution of the SW margin of the Central Anatolian Plateau, Turkey. Tectonics 31. http://dx.doi.org/10.1029/2011TC003021.

Schildgen, T.F., Cosentino, D., Bookhagen, B., Niedermann, S., Yıldırım, C., Echtler, H., Wittmann, H., Strecker, M.R., 2012b. Multi-phased uplift of the southern margin of the Central Anatolian plateau, Turkey: a record of tectonic and upper mantle processes. Earth Planet. Sci. Lett. 317–318, 85–95.

Schildgen, T.F., Yıldırım, C., Cosentino, D., Strecker, M.R., 2014. Linking slab break-off, Hellenic trench retreat, and uplift of the Central and Eastern Anatolian plateaus. Earth-Sci. Rev. 128, 147–168.

Schwartz, S.Y., Van der Voo, R., 1983. Paleomagnetic evaluation of the orocline hypothesis in the central and southern Appalachians. Geophys. Res. Lett. 10, 505–508.

Şengör, A.M.C., Yılmaz, Y., 1981. Tethyan evolution of Turkey: a plate tectonic approach. Tectonophysics 75, 181–241.

Şengör, A.M.C., Görür, N., Saroğlu, F., 1985. Strike-slip faulting and related basin formation in zones of tectonic escale: Turkey as a case study. In: Biddle, K.T., Christie-Block, N. (Eds.), Basin Formation and Sedimentation. In: Society of Economic Paleontologists and Mineralogists Special Publications, vol. 37, pp. 227–264.

Şengör, A.M.C., Özeren, S., Genç, T., Zor, E., 2003. East Anatolian high plateau as a mantle-supported, north–south shortened domal structure. Geophys. Res. Lett. 30, 8045.

Tauxe, L., Watson, G.S., 1994. The fold test: an eigen analysis approach. Earth. Planet. Sci. Lett. 122, 331–341.

Taymaz, T., Tan, O., Yolsal, S., 2004. Seismotectonics of western Turkey: a synthesis of source parameters and rupture histories of recent earthquakes. In: AGU Fall Meeting, Session T14, San Francisco–California, Eos Trans. AGU 85 (47).

Tiryakioğlu, İ., Floyd, M., Erdoğan, S., Gülal, G., Ergintav, S., McClusky, S., Reilinger, R., 2013. GPS constraints on active deformation in the Isparta Angle region of SW Turkey. Geophys. J. Int. 195, 1455–1463.

van Hinsbergen, D.J.J., 2010. A key extensional metamorphic complex reviewed and restored: the Menderes Massif of western Turkey. Earth-Sci. Rev. 102, 60–76.

van Hinsbergen, D.J.J., Schmid, S.M., 2012. Map view restoration of Aegean-West Anatolian accretion and extension since the Eocene. Tectonics 31, TC5005. http://dx.doi.org/10.1029/2012TC003132.

van Hinsbergen, D.J.J., Dekkers, M.J., Koç, A., 2010a. Testing Miocene remagnetization of Bey Dağları: timing and amount of Neogene rotations in SW Turkey. Turk. J. Earth Sci. 19, 123–156.

van Hinsbergen, D.J.J., Dekkers, M.J., Bozkurt, E., Koopman, M., 2010b. Exhumation with a twist: paleomagnetic constraints on the evolution of the Menderes metamorphic core complex (western Turkey). Tectonics 29, TC3009. http://dx.doi.org/10.1029/2009TC002596.

van Hinsbergen, D.J.J., Kaymakci, N., Spakman, W., Torsvik, T.H., 2010c. Reconciling the geological history of western Turkey with plate circuits and mantle tomography. Earth Planet. Sci. Lett. 297, 674–686.

van Velzen, A.J., Zijderveld, J.D.A., 1995. Effects of weathering on single domain magnetite in early Pliocene marls. Geophys. J. Int. 121, 267–278.

Watson, G.S., 1983. Large sample theory of the Langevin distribution. J. Stat. Plan. Inference 8, 245–256.

Wortel, M.J.R., Spakman, W., 2000. Subduction and slab detachment in the Mediterranean–Carpathian region. Science 290, 1910–1917.

Zijderveld, J.D.A., 1967. A. C. demagnetization of rocks: analysis of results. In: Collinson, D.W., Creer, K.M., Runcorn, S.K. (Eds.), Methods in Palaeomagnetism. Elsevier, Amsterdam, pp. 254–286.